Published in final edited form as:

Hum Brain Mapp. 2015 June ; 36(6): 2187–2206. doi:10.1002/hbm.22764.

Functional connectivity constrains the category-related organization of human ventral occipitotemporal cortex

W. Dale Stevens, **Michael Henry Tessler**, **Cynthia S. Peng**, and **Alex Martin**

Section on Cognitive Neuropsychology, Laboratory of Brain and Cognition, National Institute of Mental Health, National Institutes of Health, Bethesda, MD 20892, USA

Abstract

One of the most robust and oft-replicated findings in cognitive neuroscience is that several spatially distinct, functionally dissociable ventral occipitotemporal cortex (VOTC) regions respond preferentially to different categories of concrete entities. However, the determinants of this category-related organization remain to be fully determined. One recent proposal is that privileged connectivity of these VOTC regions with other regions that store and/or process category-relevant properties may be a major contributing factor. To test this hypothesis, we used a multi-category functional MRI localizer to individually define category-related brain regions of interest (ROIs) in a large group of subjects (n=33). We then used these ROIs in resting-state functional connectivity MRI analyses to explore spontaneous functional connectivity among these regions. We demonstrate that during rest, distinct category-preferential VOTC regions show differentially stronger functional connectivity with other regions that have congruent category-preference, as defined by the functional localizer. Importantly, a 'tool'-preferential region in the left medial fusiform gyrus showed differentially stronger functional connectivity with other left lateralized cortical regions associated with perceiving and knowing about common tools – posterior middle temporal gyrus (involved in perception of non-biological motion), lateral parietal cortex (critical for reaching, grasping, manipulating), and ventral premotor cortex (involved in storing/executing motor programs) – relative to other category-related regions in VOTC of both the right and left hemisphere. Our findings support the claim that privileged connectivity with other cortical regions that store and/or process category-relevant properties constrains the category-related organization of VOTC.

Keywords

fMRI; resting-state; tools; objects; scenes; PPA; hemispheric asymmetry; lateralization; concepts; localization

Corresponding Author: W. Dale Stevens, Department of Psychology, York University, Sherman Health Science Research Centre, 281 Ian Macdonald Blvd., Toronto, Ontario M3J 1P3, Canada, stevensd@yorku.ca, Phone: 416-736-2100 ext. 44662, Fax: 416-736-5772.

Conflict of Interest: The authors declare no competing financial interests

INTRODUCTION

Numerous studies have documented spatially distinct, functionally dissociable regions in human ventral occipitotemporal cortex (VOTC) that respond preferentially to different categories of concrete objects. Specifically, progressing in a lateral to medial direction along posterior VOTC, it has been repeatedly shown that viewing animate entities (full images, parts, or just the face, of people and animals) elicits greater activity in the lateral portion of the fusiform gyrus relative to viewing inanimate objects (Beauchamp et al., 2002; Kanwisher et al., 1997; McCarthy et al., 1997; Wiggett et al., 2009); viewing manipulable objects like common tools elicits greater activity in the medial portion of the fusiform gyrus relative to depictions of animate entities (Beauchamp et al., 2002; Chao et al., 1999; Weisberg et al., 2014); and viewing scenes and buildings, relative to faces and objects, elicits greater activity in a region of the posterior parahippocampal /medial fusiform gyrus (PPA) (Aguirre et al., 1998; Epstein and Kanwisher, 1998).

Various frameworks have been proposed to explain this organization, including category-dissociable eccentricity bias of visual processing – e.g., central- vs. peripheralbias for faces vs. buildings, respectively (Levy et al., 2001), real-world object size (small to large, respectively) (Konkle and Oliva, 2012), and curvature (rectilinear vs. curvilinear) (Nasr et al., 2014) (and see Malach et al., 2002; Op de Beeck et al., 2008). Although there is compelling evidence to support such bottom-up explanations, it is also clear that category-related dissociations in VOTC cannot be fully explained by appeal to these relatively low-level factors. For example, physical shape properties of objects cannot explain consistent hemispheric asymmetry of category-preferential responses (e.g., right hemisphere bias for faces in the lateral fusiform gyrus (latFG) - fusiform face area: FFA (Kanwisher et al., 1997)), nor can they explain preferential responses to categories of objects that do not share distinguishing shape or size properties, such as tools (e.g., a corkscrew vs. a broom). Thus, it is likely that other factors contribute to the topographical organization of VOTC.

Another possibility – which we will refer to here as the category-specific connectivity hypothesis – is that the category-related organization of VOTC is constrained by differential or “privileged” connectivity of specific VOTC regions with other brain regions that store and/or process category-relevant properties (Mahon and Caramazza, 2011; Mahon et al., 2007; Martin, 2006). Thus, while the organization of VOTC may be partially constrained by its connectivity with early visual cortex, it might be constrained by its connectivity with down-stream brain regions as well.

Resting-state functional connectivity (RSFC) MRI is a powerful tool for mapping functional circuits or networks across the human brain (Buckner et al., 2013; Fox and Raichle, 2007). RSFC has been shown to be functionally relevant, in that the strength of RSFC predicts individual differences in performance across a range of perceptual and cognitive tasks (e.g., Baldassarre et al., 2012; Barnes et al., 2014; Hampson et al., 2006; Koyama et al., 2011; Zhu et al., 2011). Thus, RSFC MRI is an ideal tool for testing the category-specific connectivity hypothesis.

Several studies have used RSFC MRI to explore the relationship between functional specialization and connectivity among particular brain regions – especially with regard to the PPA and FFA (Baldassano et al., 2013; He et al., 2013; Hutchison et al., 2014; O'Neil et al., 2014; Stevens et al., 2010; Stevens et al., 2012; Turk-Browne et al., 2010; Zhang et al., 2009; Zhu et al., 2011). Although these findings could be viewed as consistent with the category-specific connectivity hypothesis, their lateral (FFA) vs. medial (PPA) locations also make them consistent with the bottom up constraint of eccentricity-bias of visual processing as well.

This eccentricity bias explanation, however, cannot explain the preferential activation within medial VOTC for common tools – i.e., manmade manipulable objects for which their manner of manipulation is directly related to their function (Mahon et al., 2007). Tools would not be expected to engage periphery-biased visual processing as do large buildings or scenes, and they typically vary widely in shape, even for the same basic object category (e.g. telephones). Yet the tool-preferential VOTC ("VOTC-TOOL") region is located medially in an area that is typically associated with periphery-biased visual processing of scenes and large non-manipulable objects (e.g., buildings) near or overlapping the posterior PPA, and is typically left-lateralized (Chao et al., 1999; Garcea et al., 2012; Lewis, 2006; Mahon et al., 2007). Thus, there is no apparent link between the visual properties of tools per se, and the consistent localization of tool-preferential processing in the left medial fusiform gyrus (medFG). Viewing images of tools also engages other left-lateralized regions, including a region of the posterior middle temporal gyrus (pMTG), associated with perception of non-biological motion (Beauchamp et al., 2002); ventral premotor cortex (vPM) (Chao and Martin, 2000; Grafton et al., 1997), involved in storing and/or executing motor programs (Davare et al., 2006); and a dorsal circuit running the length of the intraparietal sulcus (IPS) extending into the anterior inferior parietal lobule (IPL), critical for spatio-motor transformations involved in reaching, grasping, and manipulation (Chao and Martin, 2000; Mruczek et al., 2013). The category-specific connectivity hypothesis would predict that the VOTC-TOOL region has differentially stronger connectivity with the aforementioned regions ("OTHER-TOOL" regions: left pMTG, IPS, IPL, and vPM) than other-category-preferring VOTC regions, including the immediately adjacent or overlapping PPA. Thus, a particularly strong test of the category-specific connectivity hypothesis would be to directly contrast the RSFC of the VOTC-TOOL region with adjacent, other-category-preferring VOTC regions, both across hemispheres, and within the same hemisphere in particular. While a few studies have explicitly investigated the RSFC of tool-related brain regions (Hutchison et al., 2014; Peelen et al., 2013; Simmons and Martin, 2012), none have demonstrated preferential connectivity of the VOTC-TOOL region with OTHER-TOOL regions, and none directly contrasted the RSFC of the VOTC-TOOL region with that of other-category-preferring VOTC regions. Thus, this critical test of the category-specific connectivity hypothesis has not previously been reported.

In this study, we used a multi-category functional MRI (fMRI) localizer to individually define multiple category-related regions of interest (ROIs), both within and outside of the VOTC, in a large group of healthy adults (n=33). We then used these ROIs in RSFC MRI analyses of high-resolution "resting-state" fMRI data to contrast the RSFC of various category-related VOTC regions with other brain regions that store and/or process category-

relevant properties. Our results provide strong evidence that functional connectivity is one of the fundamental factors that constrains the category-related topographical organization of object representations in VOTC.

MATERIALS AND METHODS

Subjects

Subjects were 33 healthy, right-handed, young adults (mean age ± standard deviation = 24.0 ± 2.3; range = 22–33; 17 females/16 males), with normal or corrected-to-normal visual acuity, no history of psychiatric, neurological, or other medical illness, or history of drug or alcohol abuse, which might compromise cognitive functions. All subjects were paid for their participation and gave written informed consent prior to participation, in accordance with a National Institutes of Health Institutional Review Board-approved protocol.

Functional localizer

During fMRI scanning, subjects completed multiple runs of a multi-category task-based functional localizer with a standard block-design task, each run consisting of 14 task blocks (20 s) interleaved with 13 fixation blocks (10s), with an additional fixation block at the beginning (18 s) and end (10 s) of the run. There were 14 different task block-types (1 of each block-type per run), consisting of 11 static image categories (tools, animals, scenes, faces, non-manipulable objects, bodies, abstract objects, words, scrambled objects, static dots, and written cues to move fingers and toes) and 3 dynamic image categories (dots moving in random motion, dots depicting biological motion, dots depicting non-biological motion; (Beauchamp et al., 2002; Beauchamp et al., 2003). Only 4 block-types of interest were included in the current study (Fig. 1): grayscale images (600 × 600 pixels) of common tools, animals, scenes (containing no animals or people), and faces (elliptically-cropped to exclude hair and clothes; half female/half male), matched in image-size to the longest dimension across all exemplars in all categories, projected onto a screen and viewed via a mirror mounted to the head coil. Each task block comprised 20 trials (stimulus duration = 300 ms; ISI = 700 ms) of a single stimulus category with either 1 or 2 stimuli repeating in immediate succession in each block. To ensure attention to each stimulus, subjects performed a repetition detection (“1-back”) task, by pressing a button with the left index finger to indicate a repetition. Each subject viewed at least 100 different exemplars in each of the 4 categories, with each exemplar repeating once throughout the entire experiment, either in immediate succession (only once or twice per block) or in separate runs.

MRI scanning

MRI data were collected using a GE Signa 3 Tesla whole-body MRI scanner with an 8-channel head coil at the NIH Clinical Center NMR Research Facility using standard procedures. For each subject, a high-resolution T1-weighted anatomical image (MRRAGE) was obtained (124 axial slices, slice thickness = 1.2 mm, Field of View (FOV) = 24 cm, acquisition matrix = 256 × 256). Spontaneously fluctuating brain activity was measured using gradient-echo echo-planar fMRI with whole-brain coverage during a “resting-state” run while subjects lay still and rested quietly while maintaining visual fixation on a centrally located white cross on a gray background (TR = 3500 ms, TE = 27 ms, flip angle = 90

degrees, 42 interleaved contiguous axial slices per volume, slice thickness = 3.0 mm, FOV = 220 mm, acquisition matrix = 128 × 128 acquisition matrix, single-voxel volume = 1.7mm × 1.7 mm × 3.0 mm). Each resting-state run lasted 8 min 10 s (140 consecutive whole-brain volumes). Next, task-evoked brain activity was similarly measured using fMRI during multiple runs of the task-based functional localizer (TR = 2000 ms, TE = 27 ms, flip angle = 77 degrees, 41 interleaved contiguous axial slices per volume, slice thickness = 3.0 mm, FOV = 216 mm, acquisition matrix = 72 × 64, single-voxel volume = 3.0mm isotropic). Each localizer run lasted 7 min 18 s (219 consecutive whole-brain volumes). Independent measures of nuisance physiological variables (cardiac and respiration) were recorded during all scans for later removal.

fMRI data preprocessing

Echo-planar images were preprocessed using the Analysis of Functional Neuroimages (AFNI) software package (Cox, 1996). For each run, the first four image-volumes were removed. Large transients in the remaining volumes were removed through interpolation (3dDespike). Volumes were then slice-time corrected (3dTshift) and co-registered to the volume nearest the anatomical scan (3dVolreg). Nuisance physiological and non-physiological artifacts were removed using a modified version of the ANATICOR procedure (Jo et al., 2010), as follows. For each subject, the anatomical scan was segmented into tissue compartments using Freesurfer (Fischl et al., 2002). Ventricle, white-matter, and draining-vessel masks were created and eroded to prevent partial volume effects with gray matter. The masks were then applied to the volume-registered echo-planar image yielding pure nuisance time-series for the ventricles and draining-vessels, as well as local estimates of the white-matter blood oxygen level-dependent (BOLD) signal averaged within a 15-mm radius sphere. Regressors for cardiac and respiratory activity were generated using Retroicor (Glover et al., 2000) and RetroTS in the AFNI Matlab library for respiration volume per time (RVT: Birn et al., 2008). Nuisance variables for each voxel's time-series included: an average ventricle time-series, an average draining-vessel time-series, a local average white-matter time-series, six head motion parameter estimates and the temporal derivative of each, and nine physiological signal regressors from Retroicor and RVT. All of the above nuisance time-series were detrended with fourth-order polynomials. Least-squares model fitted time-series of these nuisance variables were then subtracted from the voxel time-series, yielding a residual time-series that was used in all subsequent statistical analyses. These procedures have been shown to drastically reduce or virtually eliminate motion-related artifacts in resting-state time-series analyses (Jo et al., 2013). Further, this modified ANATICOR procedure eschews temporal filtering (e.g., bandpass filtering), which is ineffective at removing signals with frequencies above the Nyquist frequency (i.e., 0.5 × 1/TR ≈ 0.143 Hz in the current study) such as cardiac and respiratory signals (Gotts et al., 2013b; Van Dijk et al., 2010), and global signal regression, which can distort RSFC results in a number of detrimental ways (Gotts et al., 2013b; Murphy et al., 2009; Saad et al., 2012).

The primary purpose of the functional localizer was to independently define functional ROIs to be used in RSFC analyses of the resting-state data, the latter being of primary interest. Thus, to preserve the integrity, specificity, and high spatial resolution the resting-state data,

the localizer data were aligned to, and resampled to the resolution of the resting-state data prior to analyses and ROI definition.

For cortical surface-based analyses, subject-specific surface models were created from each subject's anatomical scan using Freesurfer. Standard-mesh surfaces of 141,000 nodes per hemisphere were created using AFNI Surface Mapper (SUMA: Saad et al., 2004) to produce node-to-node anatomical correspondence across surfaces from multiple subjects. The denoised residual time-series described above for both the localizer data and resting-state data were mapped onto the cortical surfaces (3dVol2Surf), with a mean kernel of 10 sampling points uniformly distributed along a line between smooth white matter and pial surfaces, extending 80% of the distance between corresponding nodes on the two surfaces. Spatial smoothing was performed on the surface-mapped functional data (SurfSmooth) with a heat kernel resulting in a 6 mm full-width-at-half-maximum noise spatial correlation structure along the white matter surface.

fMRI data analyses

To derive the BOLD response magnitudes for each of the conditions of interest at the individual subject level, the functional localizer data were modeled with a boxcar function, with the onset and offset points coinciding with the beginning and end of each task-block, respectively, convolved with a canonical hemodynamic response function and deconvolved using AFNI (3dDeconvolve –block). The model included 14 regressors corresponding to the 14 stimulus categories, in addition to nuisance regressors (12 regressors for the motion parameters and a third-order polynomial regressor to account for very low-frequency MRI signal drift). This analysis was conducted for both volume-based and cortical surface-based localizer data.

To test the category-specific connectivity hypothesis, we first localized the left VOTC-TOOL region in each subject based on the peak response to pictures of tools relative to animals in the localizer task data (see ROI Definition below). For each subject, we then extracted the resting-state BOLD signal time-course from the left VOTC-TOOL region to compare its RSFC with other category-related regions to that of four control VOTC regions that served different purposes: two regions in contralateral right VOTC, and two adjacent regions within left VOTC. First, we contrasted its pattern of RSFC with that of the animal-preferential right latFG (VOTC-ANIMAL) region. This latter region serves as an ideal control contrast, as tools and animals are both categories of namable entities that do not consistently differ in terms of the size or shape of objects across categories, but show robustly dissociable activation of the medial vs. lateral VOTC, respectively, and typically involve left vs. right lateralized processing, respectively (Chao et al., 1999; Garcea et al., 2012; Lewis, 2006). The second control contrast was between the left VOTC-TOOL region and the homologous region in the right medFG, to test the hypothesis that there would be category-specific hemispheric asymmetry of RSFC. The third and fourth control contrasts compared the left VOTC-TOOL region with adjacent regions in left VOTC that prefer other categories – the left VOTC-ANIMAL region in the latFG, and the left PPA (see ROI Definition below). The latter region served as a very stringent control comparison, because the location of the VOTC-TOOL region is typically overlapping or very near the location of

the PPA (Chao et al., 1999), despite the fact that tools and scenes are entirely unalike in terms of visual properties and would be expected to differentially engage center-biased vs. periphey-biased visual processing, respectively. We predicted that the left VOTC-TOOL region would show relatively stronger RSFC with other process-specific regions involved in representing information about tools (including the left pMTG, IPS, IPL, and vPM), relative to control regions in the contralateral right VOTC (right VOTC-ANIMAL and right VOTC-TOOL regions), and in adjacent regions of the left VOTC (left VOTC-ANIMAL region and left PPA). By contrast, we expected that the VOTC-ANIMAL regions would show relatively stronger RSFC with other regions important for representing information about animate entities, including other typically right lateralized regions necessary for processing faces (occipital face area: OFA, Gauthier et al., 2000), bodies (extrastriate body area: EBA, Downing et al., 2001), biological motion (posterior superior temporal sulcus: pSTS, Downing et al., 2001; Pitcher et al., 2011; Puce et al., 1998), and emotional response (amygdala: AMG, Adolphs, 1999). Finally, despite its close proximity to the VOTC-TOOL region, we expected that the left PPA would show differentially stronger RSFC with other nodes of the "scene-network", including the left and right retrosplenial complex (RSC), involved in situating scenes within their broader spatial context (Epstein, 2008), and the occipital place area (OPA; also referred to as the "transverse occipital sulcus" or "TOS"), recently shown to be selectively critical for scene processing (Dilks et al., 2013; Ganaden et al., 2013).

ROI definition

The localizer data were used to define both group-level functional ROIs and individual ROIs for each subject that were then applied to their respective resting-state data for ROI-based RSFC analyses. Standard contrasts were used to define ROIs showing category-preferential responses for different stimulus conditions. (See Table I). ROI peak activation (t-statistic) locations were defined in both surface-based and volume-based space simultaneously, using spatially locked anatomically corresponding AFNI and SUMA viewing interfaces, to cross-reference activations across viewing modalities and facilitate anatomical specificity and accuracy. ROI masks were created on the cortical surface using SUMA (ROIgrow) and included all nodes exceeding a statistical threshold of $P < 0.01$ (uncorrected) in the contrast of interest within a 6mm radius surrounding the peak (t-statistic) node within the anatomical structure of interest. Tool-preferential ROIs were defined by the contrast tools > animals, and included bilateral medFG (VOTC-TOOL: medial fusiform gyrus/sulcus-anterior lingual gyrus), left pMTG (extending from pMTG posteriorly/inferiorly into inferior temporal sulcus/gyrus), left IPS (posterior/superior), left IPL (supramarginal gyrus), and left vPM (inferior precentral gyrus extending into inferior precentral sulcus). Animal-preferential ROIs were defined by the contrast animals > tools, and included bilateral latFG, right EBA (anterior middle occipital gyrus), right pSTS, and right amygdala (activation on medial wall of cortical surface cross-referenced with amygdala activation in volume). We also analyzed RSFC of the VOTC ROIs with the OFA (inferior occipital gyrus) defined by the contrast faces > scenes, given its relevance to processing animal stimuli. Scene-preferential ROIs were defined by the contrast scenes > faces, and included the PPA (posterior parahippocampal gyrus extending posteriorly into anterior lingual gyrus), RSC (retrosplenial cortex-ventral posterior cingulate-medial parietal junction), and OPA (transverse occipital

sulcus extending into middle occipital gyrus) in both the left and right hemispheres. It is important to note that using the alternate contrast scenes > animals to define the PPA (to match the control contrast-condition to that used for defining the VOTC-TOOL region) did not significantly alter the peak PPA location across subjects – i.e., the location of peak VOTC scene response was not sensitive to the particular control contrast used (see Results). Therefore, because using different control-contrast categories (i.e., faces or animals) had no material effect on PPA localization, and because the PPA is more commonly defined by the contrast scenes > faces in previous literature, we used this contrast to define the PPA. ROI definitions and statistics are summarized in Table I.

RSFC analyses

All RSFC analyses were conducted on the cortical surface. Residual denoised BOLD signal time-series were extracted from the resting-state data by averaging across all nodes within an ROI to produce a single mean time-series for each ROI. The correlation (Pearson's *r*) between pairs of ROIs' time-series was calculated and transformed using Fisher's *z* prior to being analyzed at the group-level.

Statistical analyses

Functional localizer data were analyzed at the group level using node-wise within-subjects ANOVAs (3dANOVA). For display purposes, all contrast maps are displayed on partially inflated cortical surfaces with a statistical node-wise threshold of $P < 0.001$, whole-brain threshold of $P < 0.01$ (FDR corrected), and a minimum cluster size of 50 nodes. The ROI-based RSFC analyses were carried out using within-subjects ANOVAs on the z-transformed correlation values among pairs of ROIs' time-courses. For all "category-level analyses", the mean RSFC value of a given VOTC ROI (i.e., right or left VOTC-TOOL region, VOTC-ANIMAL region, or left PPA) with all of the other category-preferential ROIs of a given category (e.g., for tools, mean RSFC across pMTG, IPS, IPL, and vPM) was calculated to produce a mean category-level RSFC value. For analyses at the individual ROI-level, the RSFC value of a given VOTC-ROI with another individual category-preferential ROI was used in comparisons. Where predicted crossover interactions were significant, we used one-tailed paired t-tests to examine the simple main effects with the assumption of predicted direction. Otherwise, we used two-tailed paired t-tests. Error bars in all plots represent 1 between-subjects s.e.m.

RESULTS

Functional localizer

Of the 33 subjects, 26 completed all 10 runs, 5 completed 9 runs, 1 completed 8 runs, and 1 completed 6 runs. We expected that although the general topographical organization of category-related regions is broadly consistent across individuals, individual differences in the precise location of these functionally dissociable regions would be an important factor in assessing specificity of RSFC among ROIs. Thus, in addition to group-level analysis of the functional localizer data, multiple category-related ROIs were defined for each individual, both within VOTC and outside of VOTC ("OTHER" regions), on the cortical surface in their native brain space using standard functional localizer contrasts (Table I). In the group

localizer map, tool-preferential regions in VOTC were identified within the left and right medFG (VOTC-TOOL regions); those outside of VOTC ("OTHER-TOOL" regions) were left lateralized and included the pMTG, vPM, and a continuous dorsal parietal circuit running the length of the IPS, extending rostrally into the post-central sulcus, and terminating in the anterior IPL (Fig. 2A). However, at the individual-level, distinct clusters in the posterior IPS and anterior IPL (supramarginal gyrus) were most consistently observed (e.g., Fig. 5A), and as such, were considered distinct regions for the purpose of analyses. OTHER-TOOL regions were less reliably identifiable in the right than the left hemisphere across individuals, consistent with the typically observed left lateralization of tool processing, thus, ROI analyses were restricted to left hemisphere OTHER-TOOL regions (Chao et al., 1999; Garcea et al., 2012; Lewis, 2006). Animal-preferential regions in VOTC were identified within the left and right latFG (VOTC-ANIMAL regions); those outside VOTC ("OTHER-ANIMAL" regions) included bilateral EBA and AMG, and right OFA and pSTS (Fig. 2A). At the individual-level, the OTHER-ANIMAL regions were more reliably identifiable in the right hemisphere, thus, ROI analyses were restricted to the right hemisphere OTHER-ANIMAL regions. Scene-preferential regions in VOTC included the left and right PPA; those outside VOTC ("OTHER-SCENE" regions) included bilateral RSC and OPA (Fig. 2B); ROIs for all these regions were identified and defined at the individual-level (Fig. 5A). The spatial distributions of peak TOOL, ANIMAL, and SCENE activations in VOTC across subjects are displayed in Figure 3.

Because the RSFC of the left VOTC-TOOL region was compared to that of the left PPA, we determined whether the location of the left PPA differed depending on which control contrast was used (i.e., faces vs. animals). The effect of control condition was negligible: For the vast majority of subjects (26/33), the peak PPA voxel was identical or an immediately adjacent voxel; no subject had peak coordinates more than 2 voxels apart. The mean difference across the entire group in the location of each of the coordinates was: x = 0.3mm, y = 0.5mm, z = 1.2mm (i.e., less than half a single voxel width in any direction). Thus, the location of the PPA was not sensitive to which control contrast was used to define it.

Across individuals, the spatial distributions of the peak TOOL and SCENE activations in VOTC were largely overlapping (Fig. 3), and the two regions of activation were typically overlapping even at the individual level (e.g., Fig. 8a). To quantify this proximity, differences in the x-, y-, and z-coordinates of peak activation for the left VOTC-TOOL region vs. left PPA in volume-space were assessed. Paired-samples comparisons indicated that across participants, the peak coordinates of the left VOTC-TOOL region and left PPA did not significantly differ in the x-dimension (mean difference = 1.3 mm; $t_{,32} = -1.66$, $P = 0.11$, two-tailed) or y-dimension (mean difference = 2.5 mm; $t_{,32} = -1.47$, $P = 0.15$, two-tailed), but on average, the VOTC-TOOL region was slightly inferior to the PPA, as indicated by a significant difference in the z-dimension (mean difference = 3.7 mm; $t_{,32} = -4.51$, $P < 0.001$, two-tailed). Although the distribution of VOTC-TOOL peaks appears to be slightly more lateral than that of the PPA (Fig. 3), consistent with previous observations (Chao et al., 1999), this difference was not significant.

At the group-level, a direct contrast between tools and scenes revealed higher activation for scenes in the expected scene-preferential regions, including bilateral PPA, RSC, and OPA. However, although there was higher activation for tools in the expected OTHER-TOOL regions, including left pMTG, IPS, IPL, and vPM, no regions in VOTC showed higher activation for tools than for scenes at the group-level (Fig. 4), again highlighting the importance of localizing the VOTC-TOOL region at the individual level (see Mahon et al., 2007 for a similar finding).

Category-specific RSFC

For all ROI analyses, the ROI-mean BOLD time-course from the rest run was extracted from each of the individually defined VOTC ROIs, and correlated with the time-courses from all OTHER category-related ROIs. Comparisons of interest among these pairwise correlations were then conducted in ANOVAs using the Fisher's z-transformed correlation values. Predicted simple main effects were assessed with planned paired-samples comparisons (one-tailed tests were used only following significant predicted crossover interactions when there was also a strong a priori prediction of the direction of a simple main effect, otherwise two-tailed tests were used). It is important to note that the critical test of our principal hypotheses was whether or not there would be a significant VOTC-ROI by category crossover interaction in each of the category-level analyses. To foreshadow the results, there was a highly significant crossover interaction ($p < 0.001$) in the predicted direction in all three of the main analyses conducted (Fig. 5, 7, 8). The predicted interactions were also significant ($p < 0.05$) for the tests of category-specific hemispheric asymmetry of RSFC (Fig. 6). At the level of VOTC-ROI RSFC with each of the other individual category-related ROIs, although some of the individual effects were marginal or not significant, it is important to note that the overall pattern of results was highly consistent with our predictions: the vast majority of paired-samples t-tests performed were significant in the predicted direction, and not a single test performed showed a significant effect counter to our predictions (Fig. 5–8). Given the robust significance of the predicted critical interaction in every analysis we ran, and the highly consistent pattern of results for tests of the simple main effects, our results strongly confirm all of our predictions.

Differential category-specific RSFC of tool- vs. animal-preferential VOTC regions

To test the hypothesis that the left VOTC-TOOL region has relatively "privileged access" to regions that store and/or process tool-relevant properties, we first evaluated the strength of RSFC of the left VOTC-TOOL vs. the right VOTC-ANIMAL region with the OTHER-TOOL ROIs (i.e., mean RSFC with left pMTG, IPS, IPL, and vPM) vs. the OTHER-ANIMAL ROIs (i.e., mean RSFC with right OFA, EBA, pSTS, and AMG). In addition to a main effect of category ($F_{1,30} = 21.98$, $P < 0.001$; with stronger mean RSFC of the VOTC with the ANIMAL ROIs overall) we found a highly significant VOTC-ROI by category crossover interaction ($F_{1,30} = 34.05$, $P < 0.001$), characterized by stronger mean RSFC of the OTHER-TOOL regions with the left VOTC-TOOL region than the right VOTC-ANIMAL region ($t_{,30} = 1.79$, $P < 0.05$), and conversely, stronger mean RSFC of the OTHER-ANIMAL regions with the right VOTC-ANIMAL region than the left VOTC-TOOL region ($t_{,31} = -5.60$, $P < 0.001$) (Fig. 5B). In addition, significant effects were also observed for specific ROI's, with stronger RSFC of the IPS ($t_{,27} = 2.29$, $P < 0.05$), the pMTG marginally

($t_{,29} = 1.37$, $P < 0.1$), and IPL marginally ($t_{,29} = 1.52$, $P < 0.1$) with the left VOTC-TOOL region than right VOTC-ANIMAL region. Conversely, all of the OTHER-ANIMAL regions had stronger RSFC with the right VOTC-ANIMAL region than the left VOTC-TOOL region (OFA: $t_{,31} = -4.40$, $P < 0.001$; EBA: $t_{,31} = -3.80$, $P < 0.001$; pSTS: $t_{,28} = -6.28$, $P < 0.001$; AMG: $t_{,14} = -2.28$, $P < 0.05$) (Fig. 5C).

Hemispheric asymmetry of RSFC is category-specific

The previous comparison contains a possible confound of hemisphere (i.e., potentially differential strength of RSFC among ipsilateral vs. contralateral regions, independent of category-preference), inherent in the fact that both the VOTC-ROI and OTHER category-preferential regions are lateralized within the left and right hemispheres for TOOLS and ANIMALS, respectively. More importantly, this comparison does not address the critical question of whether there is category-specific hemispheric asymmetry of VOTC RSFC with OTHER category-related regions apart from a potential main effect of stronger intra- vs. inter-hemispheric RSFC. A critical aspect underlying our principal hypothesis – that RSFC with other regions that store/process category-relevant properties constrains the location of category-preferential VOTC regions – is that various functionally dissociable VOTC regions are lateralized within different hemispheres. Because the RSFC of regions involved in fine motor control (e.g., IPS, IPL, vPM) is typically left lateralized (Gotts et al., 2013a), optimally efficient connectivity (e.g., shorter path length) would bias tool perception toward left VOTC; conversely, the typically right lateralized processing of animate properties (e.g., faces and biological motion in right OFA and pSTS) would bias animal perception toward the right VOTC. Thus, we predicted stronger intra-hemispheric RSFC only among category-congruent regions, but not among category-incongruent regions. Under no circumstances would we predict stronger inter-hemispheric RSFC. If there were only a main effect of hemisphere (e.g., ipsilateral > contralateral) on RSFC strength, then one would expect stronger RSFC of the left-lateralized OTHER-TOOL regions not only with the left medFG, relative to the right medFG, but also with the left latFG relative to the right latFG; similarly, the right lateralized OTHER-ANIMAL regions would be expected to have stronger RSFC not only with the right latFG, relative to the left latFG, but also with the right medFG relative to the left medFG (i.e., hemispheric asymmetry with no category effect: Fig. 6B). However, if there were category-specific asymmetry, as predicted, then one would expect an interaction between category and hemisphere, such that the OTHER-TOOL regions would show stronger RSFC with the left medFG, relative to the right medFG, but critically, no difference in RSFC strength with the left vs. right latFG; similarly, the OTHER-ANIMAL regions would show stronger RSFC with the right latFG than the left latFG, but no difference in RSFC strength with the left vs. right medFG (i.e., category-specific hemispheric asymmetry: Fig. 6C). This prediction was confirmed by a double dissociation: there was a significant medFG-hemisphere by category interaction ($F_{1,28} = 4.67$, $P < 0.05$), with stronger mean RSFC of the OTHER-TOOL regions with the left medFG than the right medFG ($t_{,28} = 2.88$, $P < 0.01$), but critically, no difference in RSFC strength of the left vs. right medFG with the OTHER-ANIMAL regions ($t_{,30} = 0.51$, $P = 0.61$) (Fig. 6D); likewise, there was a significant latFG-hemisphere by category interaction ($F_{1,30} = 7.28$, $P < 0.05$) as predicted, with stronger mean RSFC of the OTHER-ANIMAL regions with right latFG than the left latFG ($t_{,31} = -2.66$, $P < 0.01$), but no difference in RSFC strength of the left vs. right

latFG with the OTHER-TOOL regions ($t_{30} = -0.13$, $P = 0.90$) (Fig. 6D). In addition, each of the specific OTHER-TOOL regions had stronger RSFC with the left medFG than the right medFG, including the pMTG ($t_{27} = 2.8$, $P < 0.01$), IPS ($t_{25} = 2.16$, $P < 0.05$), IPL ($t_{27} = 2.36$, $P < 0.05$), and vPM ($t_{25} = 1.93$, $P = 0.05$), but none of these regions had differential RSFC with the left vs. right latFG (Fig. 6E, left). Conversely, only OTHER-ANIMAL regions had stronger RSFC with the right latFG than the left latFG, including the OFA ($t_{31} = -2.28$, $P < 0.05$), EBA ($t_{31} = -1.95$, $P = 0.05$), and AMG ($t_{14} = -2.04$, $P < 0.05$), but none showed differential RSFC with the right vs. left medFG (Fig. 6E, right). Thus, consistent with our predictions, we observed stronger intra-hemispheric RSFC only among category-congruent regions, but not among category-incongruent regions.

Category dissociations within left VOTC are associated with differential RSFC

Finally, to more directly test the category specificity of RSFC of the left medFG, we contrasted RSFC of the left VOTC-TOOL region with the OTHER-TOOL regions, relative to two other category-related areas in same hemisphere (left VOTC); the adjacent VOTC-ANIMAL region (in left latFG) and the left PPA. Comparison of the adjacent lateral and medial regions of the left fusiform gyrus yielded a VOTC-ROI by category crossover interaction ($F_{1,30} = 13.01$, $P < 0.001$), with marginally stronger mean RSFC of the OTHER-TOOL regions with the left VOTC-TOOL region than the left VOTC-ANIMAL region ($t_{30} = 1.50$, $P = 0.07$), and conversely, stronger mean RSFC of the OTHER-ANIMAL regions with the left VOTC-ANIMAL region than the left VOTC-TOOL region ($t_{31} = -2.85$, $P < 0.01$) (Fig. 7B). For specific ROIs, only OTHER-TOOL regions had stronger RSFC with the left VOTC-TOOL region than the left VOTC-ANIMAL region, including the IPS ($t_{27} = 2.11$, $P < 0.05$), IPL ($t_{29} = 1.85$, $P < 0.05$), and pMTG marginally ($t_{29} = 1.35$, $P < 0.1$). Conversely, only OTHER-ANIMAL regions had stronger RSFC with the left VOTC-ANIMAL region than the left VOTC-TOOL region, including the OFA ($t_{31} = -1.91$, $P < 0.05$), pSTS ($t_{28} = -3.75$, $P < 0.001$), and EBA marginally ($t_{31} = -1.35$, $P < 0.1$) (Fig. 7C).

Similarly, comparison of the left VOTC-TOOL region vs. left PPA yielded a significant VOTC-ROI by category crossover interaction ($F_{1,30} = 42.01$, $P < 0.001$), with relatively stronger mean RSFC of the OTHER-TOOL regions with the VOTC-TOOL region than the PPA ($t_{30} = 2.60$, $P < 0.01$), and conversely, stronger mean RSFC of the OTHER-SCENE regions with the PPA than the VOTC-TOOL region ($t_{32} = -4.56$, $P < 0.001$) (Fig. 8C). For specific ROI's, only OTHER-TOOL regions had stronger RSFC with the VOTC-TOOL region than the PPA, including the IPS ($t_{27} = 3.95$, $P < 0.001$) and IPL ($t_{29} = 2.21$, $P < 0.05$). Conversely, only OTHER-SCENE regions had stronger RSFC with the PPA than the VOTC-TOOL region, including the left RSC ($t_{32} = -4.27$, $P < 0.001$), right RSC ($t_{32} = -4.68$, $P < 0.001$), and left OPA ($t_{32} = -1.83$, $P < 0.05$) (Fig. 8D).

DISCUSSION

By combining individual functional localization of multiple category-preferential regions with RSFC MRI analyses of independent resting-state data, we demonstrated that distinct category-preferential regions in VOTC have differentially stronger intrinsic connectivity with other cortical regions that store and/or process their respective category-relevant

properties. Most importantly, by using individually defined category-related ROIs in VOTC, we were able to document differentially stronger RSFC between the tool-related ROI located in the medial region of the fusiform gyrus and several other well-known left hemisphere regions associated with perceiving and knowing about tools (pMTG, IPS, IPL, and vPM), relative to four other category-preferential VOTC regions; the homologous region in the right medFG (critically, showing category-specific hemispheric asymmetry), the contralateral right latFG region associated with viewing animals, as well as the adjacent left latFG region, and the immediately adjacent and overlapping left PPA. By contrast, the latFG regions showed relatively stronger RSFC with regions typically associated with viewing animate entities, while the PPA showed stronger RSFC with nodes of the scene-network. Taken together, these results provide strong support for the hypothesis that the category-related topographical organization of human VOTC is constrained by intrinsic connectivity with other regions that store and/or process category-relevant properties.

Our results are consistent with other work that has used RSFC to demonstrate preferential connectivity among brain regions that show congruent category-preferential responses (faces and scenes: (He et al., 2013; Hutchison et al., 2014; O'Neil et al., 2014; Stevens et al., 2010; Stevens et al., 2012; Turk-Browne et al., 2010; Zhang et al., 2009; Zhu et al., 2011); objects and bodies: (Hutchison et al., 2014)). However, as set forth in the Introduction, exploring the connectivity of the VOTC-TOOL region in particular is a critical test of the category-specific connectivity hypothesis, given that its location is not consistent with other explanations of category-related VOTC organization. Although as mentioned previously, several studies have evaluated intrinsic functional connectivity of regions associated with tools (Hutchison et al., 2014; Peelen et al., 2013; Simmons and Martin, 2012), none have shown preferential RSFC of the VOTC-TOOL region with other tool-preferential regions, and critically, none directly contrasted or showed differential patterns of RSFC of the VOTC-TOOL region relative to other category-preferential VOTC regions within or across hemispheres. Our success in doing so may have resulted from defining the category-related ROIs individually in each subject, in contrast to using a single group-defined coordinate as done in the above noted studies. Previous work has shown that localizing category-preferential VOTC regions in each individual is critical for evaluating task-based functional dissociations (e.g., Glezer and Riesenhuber, 2013) and the same may hold for evaluating RSFC as well.

An important and fundamental issue to resolve is whether connectivity actually drives (at least in part) category-related organization, or whether functional specialization of particular VOTC regions is primary, existing independent of category-specific connectivity, which only emerges later. Our finding of category-specific hemispheric asymmetry of the RSFC of the VOTC-TOOL region provides some evidence in favor of the former possibility. A recent study using RFSC to explore brain-wide hemispheric functional asymmetry demonstrated that the left hemisphere shows a relative bias for intra-hemispheric interaction, particularly for regions involved in language and fine motor control, while right hemisphere regions involved in visuospatial and attentional processing show a bias for inter-hemispheric integration (Gotts et al., 2013a); see also (Liu et al., 2009). There is no obvious reason to expect that visual properties alone could lead to lateralized representation or processing in VOTC. However, if optimally efficient connectivity (e.g., shorter path length) with left

lateralized regions involved in fine motor control plays a role in determining which region of VOTC is most involved in perceiving tools, this would explain why tool-related processing in VOTC is left lateralized. By contrast, a region such as the PPA involved in spatial perception/navigation broadly across visual fields would benefit from interconnectivity across hemispheres, resulting in bilateral representation and connectivity, as has been typically observed. In another recent study, Wang et al. (2014) reported that whereas heteromodal/association cortices show prominent hemispheric specialization (i.e., stronger within- than cross-hemispheric RSFC), unimodal/sensorimotor cortices show minimal hemispheric specialization. Further, the degree of hemispheric specialization across the cortex was correlated with the degree of evolutionary expansion of these regions. It is interesting to note that the left lateralized regions in the current study associated with tool perception, a more evolutionarily advanced ability, generally align with regions showing a higher degree of both hemispheric specialization and evolutionary cortical expansion (e.g., posterior lateral parietal cortex, posterior lateral temporal cortex, ventral premotor cortex); conversely, the bilateral regions associated with scene perception, an evolutionarily more primitive ability, align with regions showing minimal hemispheric specialization and cortical expansion (e.g., lateral occipital and retrosplenial cortex) (cf. Wang et al., 2014).

Across comparisons, left lateral parietal cortex consistently showed the most prominent and reliable specificity of RSFC with the left VOTC-TOOL region. The functional localizer revealed higher activation for tools relative to animals throughout a continuous dorsal circuit extending from the posterior IPS into the anterior IPL at the group level, and typically in two distinct regions at the individual level – one, more posterior/superior in IPS, and the other, more anterior/inferior in IPL. These results were consistent with a recent study by Mruczek et al. (Mruczek et al., 2013) that reported a highly detailed analysis of tool-related responses along the length of this circuit. While the entire circuit showed a tool-preferential response (relative to animals), there was a posterior-to-anterior decreasing response gradient to graspable non-tool objects. Thus, our IPS and IPL regions most likely map onto regions primarily involved in grasping vs. manipulation, respectively. Mahon and colleagues (Almeida et al., 2013; Garcea and Mahon, 2014; Mahon et al., 2013) have also reported similar dissociations within lateral parietal cortex. They demonstrated a dissociation between a more inferior parietal region that responds preferentially only to high spatial frequency images of tools vs. a more superior parietal region that responds preferentially only to low spatial frequency images of tools, which were presumed to be regions associated with manipulation vs. grasping, respectively (Mahon et al., 2013; see also Almeida et al., 2013). They argued that because the dorsal stream is driven largely by magnocellular input that is biased toward low spatial frequency visual information, tool-preferential responses to high spatial frequency images in the inferior parietal region indicated inputs form the ventral visual pathway. Analyses of functional connectivity in task data (block design; animals and tools) suggest that an inferior parietal region shows relatively stronger functional connectivity with the left medFG relative to a more posterior/superior parietal region (Almeida et al., 2013; Garcea and Mahon, 2014; Mahon et al., 2013). However, they did not demonstrate differential connectivity of the VOTC-TOOL region relative to any other category-related VOTC regions. On the face if it, and on the assumption that there is some correspondence between the inferior/anterior/manipulation vs. posterior/superior/grasping

regions across studies, the latter results appear to conflict with our results. Here, the RSFC of the VOTC-TOOL region with the IPS was as strong as, if not stronger than, any of the multiple other regions assessed in the current study, including the more anterior/inferior IPL. However it is important to note several fundamental differences between the current and previous analyses. Whereas the current study assessed spontaneous functional connectivity using RSFC in independent rest data, the studies by Mahon and colleagues assessed correlations among regions in task data that included multiple tool-blocks alternating with animal- and fixation-blocks, thus the effects are most likely driven primarily by the ongoing task-related activity. Further, the ROIs used in those analyses were based on a single set of coordinates defined at the group level, or based on previous literature, as opposed to individually localized as was done here, which could have an impact on the results. Importantly, parietal regions in the current study were defined only by the contrast TOOL > ANIMAL, thus it is uncertain whether the IPL and IPS regions reported here specifically correspond to manipulation vs. grasping regions and/or high vs. low spatial frequency responsive regions. An important direction for future research will be to further assess differential connectivity of the multiple functionally dissociable parietal regions with various VOTC regions and other regions of the brain using RSFC.

In the current study, the category-specific connectivity hypothesis was tested exclusively using measures of functional connectivity with RSFC MRI. An important topic is the extent to which RSFC reflects, interacts with, or even has a causal effect on structural brain connectivity. One of the most striking findings was the robust difference in the strength of RSFC of the IPS and IPL with the VOTC-TOOL region relative to the immediately adjacent or overlapping PPA. This finding fits well with a recently proposed new neural framework of visuospatial processing, based on neuroanatomy of the macaque monkey, demonstrating that the parietal component of the dorsal visual stream trifurcates into three distinct pathways that mediate both spatial perception and visually guided action across multiple cortical areas (Kravitz et al., 2011). One of these primary pathways projects from the caudal IPL (cIPL) to the medial temporal lobe via two distinct routes: one that courses directly from the cIPL and terminates in the posterior parahippocampal region, and a second one with the same source and targets that courses indirectly through the posterior cingulate and retrosplenial areas (Kravitz et al., 2011). It is interesting to speculate that these two sub-pathways, the direct and the indirect, might terminate in very anatomically close yet distinct regions, giving rise to tool-preferential (VOTC-TOOL region) vs. scene-preferential (PPA) regions, respectively. This could explain the stronger RSFC of the VOTC-TOOL region with left parietal regions via the direct pathway, vs. the PPA that showed stronger RSFC with the RSC, which comprises retrosplenial and posterior cingulate cortex (Epstein, 2008).

It has been shown that while patterns of RSFC are constrained to a large extent by anatomical connectivity (Hermundstad et al., 2013; Honey et al., 2010), they are also strong among nodes of functionally defined networks (Greicius et al., 2003; Simmons and Martin, 2012; Spreng et al., 2013; Spreng et al., 2010; Turk-Browne et al., 2010; Vincent et al., 2008; Zhang et al., 2009), are subtly modulated by recent or ongoing experience in functionally relevant networks (Albert et al., 2009; Gordon et al., 2012; Grigg and Grady, 2010; Hasson et al., 2009; Lewis et al., 2009; Stevens et al., 2010; Tambini et al., 2010; Tung et al., 2013; Waites et al., 2005), predict individual differences in task performance

(Baldassarre et al., 2012; Barnes et al., 2014; Hampson et al., 2006; Koyama et al., 2011; O'Neil et al., 2014; Zhu et al., 2011), and play a role in learning and memory (Lewis et al., 2009; Stevens et al., 2010; Tambini et al., 2010). Thus, RSFC among brain regions is malleable, and may strengthen over time in an experience-dependent manner, through a history of repeated coupling of activity driven by cognitive processing, which facilitates future performance, reflecting a Hebbian-like mechanism (Dosenbach et al., 2007; Lewis et al., 2009; Stevens and Spreng, 2014) involved in the developmental specialization of category-specific cortical circuits. We propose that such a mechanism might play a fundamental role in the development of category-related organization of VOTC, and therefore that RSFC MRI is an ideal tool for testing the category-specific connectivity hypothesis. An important direction for future work will be investigating the possibility that repeated modulation of RSFC on relatively short timescales might be relevant or causally related to the much slower anatomical changes associated with training, development, and evolution.

Acknowledgements

This study was supported by the National Institute of Mental Health, National Institutes of Health, Division of Intramural Research. The authors thank Ziad Saad, Bob Cox, and Daniel Glen for invaluable assistance with AFNI and SUMA analyses; Steve Gotts, Kelley Barnes, Chris Baker, and Dwight Kravitz for helpful discussions; and members of the Laboratory of Brain and Cognition, NIMH, for helpful feedback and discussions.

REFERENCES

Adolphs R. Social cognition and the human brain. Trends Cogn Sci. 1999; 3(12):469–479. [PubMed: 10562726]

Aguirre GK, Zarahn E, D'Esposito M. An area within human ventral cortex sensitive to "building" stimuli: evidence and implications. Neuron. 1998; 21(2):373–383. [PubMed: 9728918]

Albert NB, Robertson EM, Miall RC. The resting human brain and motor learning. Curr Biol. 2009; 19(12):1023–1027. [PubMed: 19427210]

Almeida J, Fintzi AR, Mahon BZ. Tool manipulation knowledge is retrieved by way of the ventral visual object processing pathway. Cortex. 2013; 49(9):2334–2344. [PubMed: 23810714]

Baldassano C, Beck DM, Fei-Fei L. Differential connectivity within the Parahippocampal Place Area. Neuroimage. 2013; 75:228–237. [PubMed: 23507385]

Baldassarre A, Lewis CM, Committeri G, Snyder AZ, Romani GL, Corbetta M. Individual variability in functional connectivity predicts performance of a perceptual task. Proc Natl Acad Sci U S A. 2012; 109(9):3516–3521. [PubMed: 22315406]

Barnes KA, Anderson KM, Plitt M, Martin A. Individual differences in intrinsic brain connectivity predict decision strategy. J Neurophysiol. 2014

Beauchamp MS, Lee KE, Haxby JV, Martin A. Parallel visual motion processing streams for manipulable objects and human movements. Neuron. 2002; 34(1):149–159. [PubMed: 11931749]

Beauchamp MS, Lee KE, Haxby JV, Martin A. FMRI responses to video and point-light displays of moving humans and manipulable objects. J Cogn Neurosci. 2003; 15(7):991–1001. [PubMed: 14614810]

Birn RM, Smith MA, Jones TB, Bandettini PA. The respiration response function: the temporal dynamics of fMRI signal fluctuations related to changes in respiration. Neuroimage. 2008; 40(2): 644–654. [PubMed: 18234517]

Buckner RL, Krienen FM, Yeo BT. Opportunities and limitations of intrinsic functional connectivity MRI. Nat Neurosci. 2013; 16(7):832–837. [PubMed: 23799476]

Chao LL, Haxby JV, Martin A. Attribute-based neural substrates in temporal cortex for perceiving and knowing about objects. Nat Neurosci. 1999; 2(10):913–919. [PubMed: 10491613]

Chao LL, Martin A. Representation of manipulable man-made objects in the dorsal stream. Neuroimage. 2000; 12(4):478–484. [PubMed: 10988041]

Cox RW. AFNI: software for analysis and visualization of functional magnetic resonance neuroimages. Comput Biomed Res. 1996; 29(3):162–173. [PubMed: 8812068]

Davare M, Andres M, Cosnard G, Thonnard JL, Olivier E. Dissociating the role of ventral and dorsal premotor cortex in precision grasping. J Neurosci. 2006; 26(8):2260–2268. [PubMed: 16495453]

Dilks DD, Julian JB, Paunov AM, Kanwisher N. The occipital place area is causally and selectively involved in scene perception. J Neurosci. 2013; 33(4):1331a–1336a. [PubMed: 23345209]

Dosenbach NU, Fair DA, Miezin FM, Cohen AL, Wenger KK, Dosenbach RA, Fox MD, Snyder AZ, Vincent JL, Raichle ME, et al. Distinct brain networks for adaptive and stable task control in humans. Proc Natl Acad Sci U S A. 2007; 104(26):11073–11078. [PubMed: 17576922]

Downing PE, Jiang Y, Shuman M, Kanwisher N. A cortical area selective for visual processing of the human body. Science. 2001; 293(5539):2470–2473. [PubMed: 11577239]

Epstein R, Kanwisher N. A cortical representation of the local visual environment. Nature. 1998; 392(6676):598–601. [PubMed: 9560155]

Epstein RA. Parahippocampal and retrosplenial contributions to human spatial navigation. Trends Cogn Sci. 2008; 12(10):388–396. [PubMed: 18760955]

Fischl B, Salat DH, Busa E, Albert M, Dieterich M, Haselgrove C, van der Kouwe A, Killiany R, Kennedy D, Klaveness S, et al. Whole brain segmentation: automated labeling of neuroanatomical structures in the human brain. Neuron. 2002; 33(3):341–355. [PubMed: 11832223]

Fox MD, Raichle ME. Spontaneous fluctuations in brain activity observed with functional magnetic resonance imaging. Nat Rev Neurosci. 2007; 8(9):700–711. [PubMed: 17704812]

Ganaden RE, Mullin CR, Steeves JK. Transcranial magnetic stimulation to the transverse occipital sulcus affects scene but not object processing. J Cogn Neurosci. 2013; 25(6):961–968. [PubMed: 23410031]

Garcea FE, Almeida J, Mahon BZ. A right visual field advantage for visual processing of manipulable objects. Cogn Affect Behav Neurosci. 2012; 12(4):813–825. [PubMed: 22864955]

Garcea FE, Mahon BZ. Parcellation of left parietal tool representations by functional connectivity. Neuropsychologia. 2014; 60:131–143. [PubMed: 24892224]

Gauthier I, Tarr MJ, Moylan J, Skudlarski P, Gore JC, Anderson AW. The fusiform "face area" is part of a network that processes faces at the individual level. J Cogn Neurosci. 2000; 12(3):495–504. [PubMed: 10931774]

Glezer LS, Riesenhuber M. Individual variability in location impacts orthographic selectivity in the "visual word form area". J Neurosci. 2013; 33(27):11221–11226. [PubMed: 23825425]

Glover GH, Li TQ, Ress D. Image-based method for retrospective correction of physiological motion effects in fMRI: RETROICOR. Magn Reson Med. 2000; 44(1):162–167. [PubMed: 10893535]

Gordon EM, Breeden AL, Bean SE, Vaidya CJ. Working memory-related changes in functional connectivity persist beyond task disengagement. Hum Brain Mapp. 2012

Gotts SJ, Jo HJ, Wallace GL, Saad ZS, Cox RW, Martin A. Two distinct forms of functional lateralization in the human brain. Proc Natl Acad Sci U S A. 2013a; 110(36):E3435–E3444. [PubMed: 23959883]

Gotts SJ, Saad ZS, Jo HJ, Wallace GL, Cox RW, Martin A. The perils of global signal regression for group comparisons: a case study of Autism Spectrum Disorders. Front Hum Neurosci. 2013b; 7:356. [PubMed: 23874279]

Grafton ST, Fadiga L, Arbib MA, Rizzolatti G. Premotor cortex activation during observation and naming of familiar tools. Neuroimage. 1997; 6(4):231–236. [PubMed: 9417966]

Greicius MD, Krasnow B, Reiss AL, Menon V. Functional connectivity in the resting brain: a network analysis of the default mode hypothesis. Proc Natl Acad Sci U S A. 2003; 100(1):253–258. [PubMed: 12506194]

Grigg O, Grady CL. Task-related effects on the temporal and spatial dynamics of resting-state functional connectivity in the default network. PLoS One. 2010; 5(10):e13311. [PubMed: 20967203]

Hampson M, Driesen NR, Skudlarski P, Gore JC, Constable RT. Brain connectivity related to working memory performance. J Neurosci. 2006; 26(51):13338–13343. [PubMed: 17182784]

Hasson U, Nusbaum HC, Small SL. Task-dependent organization of brain regions active during rest. Proc Natl Acad Sci U S A. 2009; 106(26):10841–10846. [PubMed: 19541656]

He C, Peelen MV, Han Z, Lin N, Caramazza A, Bi Y. Selectivity for large nonmanipulable objects in scene-selective visual cortex does not require visual experience. Neuroimage. 2013; 79:1–9. [PubMed: 23624496]

Hermundstad AM, Bassett DS, Brown KS, Aminoff EM, Clewett D, Freeman S, Frithsen A, Johnson A, Tipper CM, Miller MB, et al. Structural foundations of resting-state and task-based functional connectivity in the human brain. Proc Natl Acad Sci U S A. 2013; 110(15):6169–6174. [PubMed: 23530246]

Honey CJ, Thivierge JP, Sporns O. Can structure predict function in the human brain? Neuroimage. 2010; 52(3):766–776. [PubMed: 20116438]

Hutchison RM, Culham JC, Everling S, Flanagan JR, Gallivan JP. Distinct and distributed functional connectivity patterns across cortex reflect the domain-specific constraints of object, face, scene, body, and tool category-selective modules in the ventral visual pathway. Neuroimage. 2014; 96:216–236. [PubMed: 24699018]

Jo HJ, Gotts SJ, Reynolds RC, Bandettini PA, Martin A, Cox RW, Saad ZS. Effective Preprocessing Procedures Virtually Eliminate Distance-Dependent Motion Artifacts in Resting State FMRI. J Appl Math. 2013; 2013

Jo HJ, Saad ZS, Simmons WK, Milbury LA, Cox RW. Mapping sources of correlation in resting state FMRI, with artifact detection and removal. Neuroimage. 2010; 52(2):571–582. [PubMed: 20420926]

Kanwisher N, McDermott J, Chun MM. The fusiform face area: a module in human extrastriate cortex specialized for face perception. J Neurosci. 1997; 17(11):4302–4311. [PubMed: 9151747]

Konkle T, Oliva A. A real-world size organization of object responses in occipitotemporal cortex. Neuron. 2012; 74(6):1114–1124. [PubMed: 22726840]

Koyama MS, Di Martino A, Zuo XN, Kelly C, Mennes M, Jutagir DR, Castellanos FX, Milham MP. Resting-state functional connectivity indexes reading competence in children and adults. J Neurosci. 2011; 31(23):8617–8624. [PubMed: 21653865]

Kravitz DJ, Saleem KS, Baker CI, Mishkin M. A new neural framework for visuospatial processing. Nat Rev Neurosci. 2011; 12(4):217–230. [PubMed: 21415848]

Levy I, Hasson U, Avidan G, Hendler T, Malach R. Center-periphery organization of human object areas. Nat Neurosci. 2001; 4(5):533–539. [PubMed: 11319563]

Lewis CM, Baldassarre A, Committeri G, Romani GL, Corbetta M. Learning sculpts the spontaneous activity of the resting human brain. Proc Natl Acad Sci U S A. 2009; 106(41):17558–17563. [PubMed: 19805061]

Lewis JW. Cortical networks related to human use of tools. Neuroscientist. 2006; 12(3):211–231. [PubMed: 16684967]

Liu H, Stufflebeam SM, Sepulcre J, Hedden T, Buckner RL. Evidence from intrinsic activity that asymmetry of the human brain is controlled by multiple factors. Proc Natl Acad Sci U S A. 2009; 106(48):20499–20503. [PubMed: 19918055]

Mahon BZ, Caramazza A. What drives the organization of object knowledge in the brain? Trends Cogn Sci. 2011; 15(3):97–103. [PubMed: 21317022]

Mahon BZ, Kumar N, Almeida J. Spatial frequency tuning reveals interactions between the dorsal and ventral visual systems. J Cogn Neurosci. 2013; 25(6):862–871. [PubMed: 23410033]

Mahon BZ, Milleville SC, Negri GA, Rumiati RI, Caramazza A, Martin A. Action-related properties shape object representations in the ventral stream. Neuron. 2007; 55(3):507–520. [PubMed: 17678861]

Malach R, Levy I, Hasson U. The topography of high-order human object areas. Trends Cogn Sci. 2002; 6(4):176–184. [PubMed: 11912041]

Martin A. Shades of Dejerine--forging a causal link between the visual word form area and reading. Neuron. 2006; 50(2):173–175. [PubMed: 16630825]

McCarthy G, Puce A, Gore JC, Allison T. Face-specific processing in the human fusiform gyrus. J Cogn Neurosci. 1997; 9(5):605–610. [PubMed: 23965119]

Mruczek RE, von Loga IS, Kastner S. The representation of tool and non-tool object information in the human intraparietal sulcus. J Neurophysiol. 2013; 109(12):2883–2896. [PubMed: 23536716]

Murphy K, Birn RM, Handwerker DA, Jones TB, Bandettini PA. The impact of global signal regression on resting state correlations: are anti-correlated networks introduced? Neuroimage. 2009; 44(3):893–905. [PubMed: 18976716]

Nasr S, Echavarria CE, Tootell RB. Thinking outside the box: rectilinear shapes selectively activate scene-selective cortex. J Neurosci. 2014; 34(20):6721–6735. [PubMed: 24828628]

O'Neil EB, Hutchison RM, McLean DA, Kohler S. Resting-state fMRI reveals functional connectivity between face-selective perirhinal cortex and the fusiform face area related to face inversion. Neuroimage. 2014; 92C:349–355. [PubMed: 24531049]

Op de Beeck HP, Dicarlo JJ, Goense JB, Grill-Spector K, Papanastassiou A, Tanifuji M, Tsao DY. Fine-scale spatial organization of face and object selectivity in the temporal lobe: do functional magnetic resonance imaging, optical imaging, and electrophysiology agree? J Neurosci. 2008; 28(46):11796–11801. [PubMed: 19005042]

Peelen MV, Bracci S, Lu X, He C, Caramazza A, Bi Y. Tool selectivity in left occipitotemporal cortex develops without vision. J Cogn Neurosci. 2013; 25(8):1225–1234. [PubMed: 23647514]

Pitcher D, Dilks DD, Saxe RR, Triantafyllou C, Kanwisher N. Differential selectivity for dynamic versus static information in face-selective cortical regions. Neuroimage. 2011; 56(4):2356–2363. [PubMed: 21473921]

Puce A, Allison T, Bentin S, Gore JC, McCarthy G. Temporal cortex activation in humans viewing eye and mouth movements. J Neurosci. 1998; 18(6):2188–2199. [PubMed: 9482803]

Saad ZS, Gotts SJ, Murphy K, Chen G, Jo HJ, Martin A, Cox RW. Trouble at rest: how correlation patterns and group differences become distorted after global signal regression. Brain Connect. 2012; 2(1):25–32. [PubMed: 22432927]

Saad, ZS.; Reynolds, RC.; Argall, RC.; Japee, S.; Cox, RW. SUMA: An interface for surface-based intra- and inter-subject analysis with AFN. Arlington, VA: Institute of Electrical and Electronic Engineers; 2004. p. 1510-1513.

Simmons WK, Martin A. Spontaneous resting-state BOLD fluctuations reveal persistent domain-specific neural networks. Soc Cogn Affect Neurosci. 2012; 7(4):467–475. [PubMed: 21586527]

Spreng RN, Sepulcre J, Turner GR, Stevens WD, Schacter DL. Intrinsic architecture underlying the relations among the default, dorsal attention, and frontoparietal control networks of the human brain. J Cogn Neurosci. 2013; 25(1):74–86. [PubMed: 22905821]

Spreng RN, Stevens WD, Chamberlain JP, Gilmore AW, Schacter DL. Default network activity, coupled with the frontoparietal control network, supports goal-directed cognition. Neuroimage. 2010; 53(1):303–317. [PubMed: 20600998]

Stevens WD, Buckner RL, Schacter DL. Correlated low-frequency BOLD fluctuations in the resting human brain are modulated by recent experience in category-preferential visual regions. Cereb Cortex. 2010; 20(8):1997–2006. [PubMed: 20026486]

Stevens WD, Kahn I, Wig GS, Schacter DL. Hemispheric asymmetry of visual scene processing in the human brain: evidence from repetition priming and intrinsic activity. Cereb Cortex. 2012; 22(8): 1935–1949. [PubMed: 21968568]

Stevens WD, Spreng RN. Resting-state functional connectivity MRI reveals active processes central to cognition. Wiley Interdisciplinary Reviews-Cognitive Science. 2014; 5(2):233–245.

Tambini A, Ketz N, Davachi L. Enhanced brain correlations during rest are related to memory for recent experiences. Neuron. 2010; 65(2):280–290. [PubMed: 20152133]

Tung KC, Uh J, Mao D, Xu F, Xiao G, Lu H. Alterations in resting functional connectivity due to recent motor task. Neuroimage. 2013; 78:316–324. [PubMed: 23583747]

Turk-Browne NB, Norman-Haignere SV, McCarthy G. Face-Specific Resting Functional Connectivity between the Fusiform Gyrus and Posterior Superior Temporal Sulcus. Front Hum Neurosci. 2010; 4:176. [PubMed: 21151362]

Van Dijk KR, Hedden T, Venkataraman A, Evans KC, Lazar SW, Buckner RL. Intrinsic functional connectivity as a tool for human connectomics: theory, properties, and optimization. J Neurophysiol. 2010; 103(1):297–321. [PubMed: 19889849]

Vincent JL, Kahn I, Snyder AZ, Raichle ME, Buckner RL. Evidence for a frontoparietal control system revealed by intrinsic functional connectivity. J Neurophysiol. 2008; 100(6):3328–3342. [PubMed: 18799601]

Waites AB, Stanislavsky A, Abbott DF, Jackson GD. Effect of prior cognitive state on resting state networks measured with functional connectivity. Hum Brain Mapp. 2005; 24(1):59–68. [PubMed: 15382248]

Wang D, Buckner RL, Liu H. Functional specialization in the human brain estimated by intrinsic hemispheric interaction. J Neurosci. 2014; 34(37):12341–12352. [PubMed: 25209275]

Weisberg J, Milleville SC, Kenworthy L, Wallace GL, Gotts SJ, Beauchamp MS, Martin A. Social perception in autism spectrum disorders: impaired category selectivity for dynamic but not static images in ventral temporal cortex. Cereb Cortex. 2014; 24(1):37–48. [PubMed: 23019245]

Wiggett AJ, Pritchard IC, Downing PE. Animate and inanimate objects in human visual cortex: Evidence for task-independent category effects. Neuropsychologia. 2009; 47(14):3111–3117. [PubMed: 19631673]

Zhang H, Tian J, Liu J, Li J, Lee K. Intrinsically organized network for face perception during the resting state. Neurosci Lett. 2009; 454(1):1–5. [PubMed: 19429043]

Zhu Q, Zhang J, Luo YL, Dilks DD, Liu J. Resting-state neural activity across face-selective cortical regions is behaviorally relevant. J Neurosci. 2011; 31(28):10323–10330. [PubMed: 21753009]

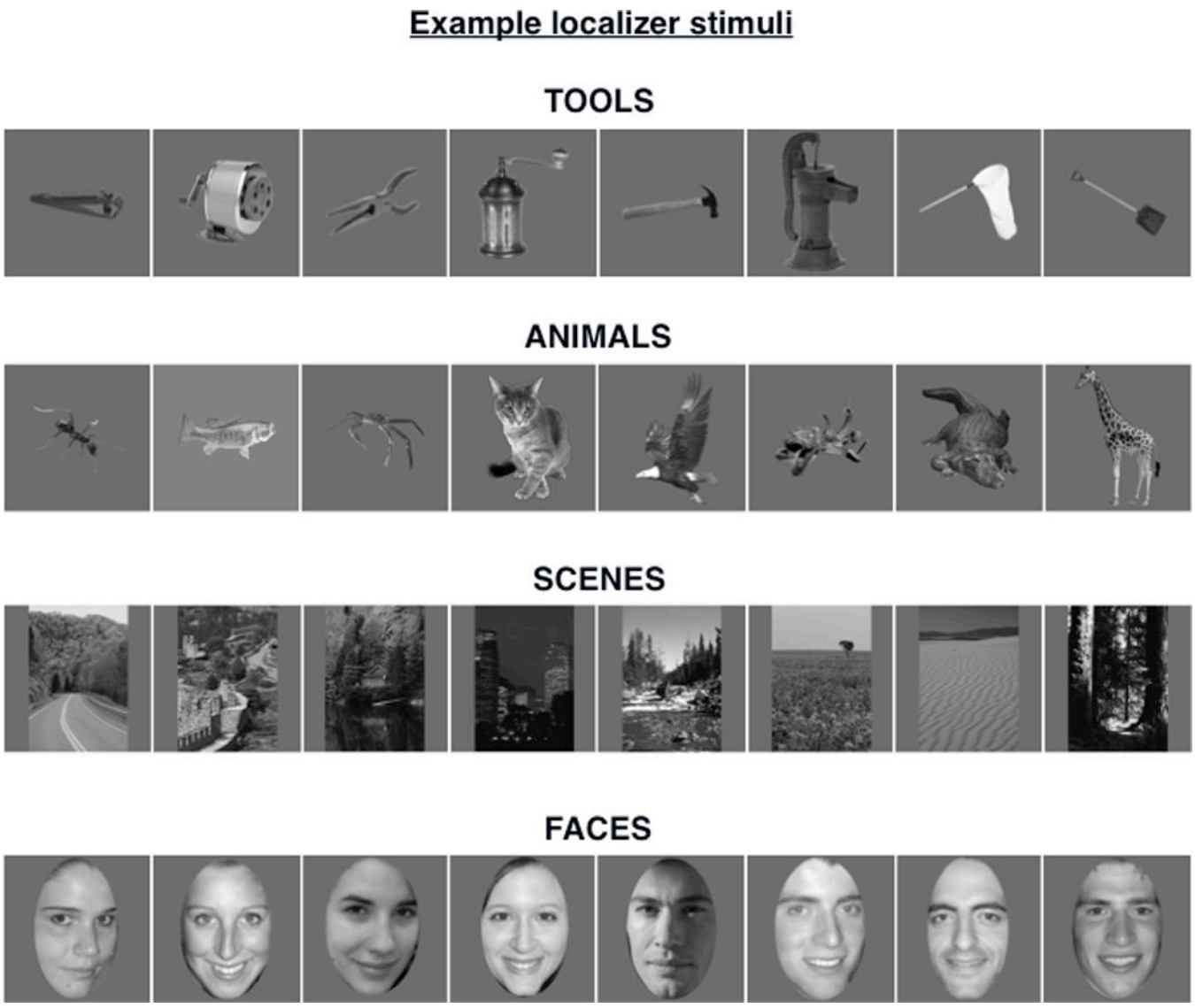

Figure 1.

Example stimuli from the functional localizer. TOOLS ranged in real-world size and function; examples arranged from left to right in ascending order of real-world size, including the smallest (left) and largest (right) exemplars. ANIMALS included exemplars from multiple classes of vertebrates and invertebrates; examples arranged from left to right in ascending order of real-world size, including the smallest (left) and largest (right) exemplars. SCENES were outdoors; included no animals, people, or tools; half "man-made" (left), half "natural" (right). FACES had neutral-to-positive expressions; elliptically cropped to exclude clothing and as much hair as possible; half female (left), half male (right).

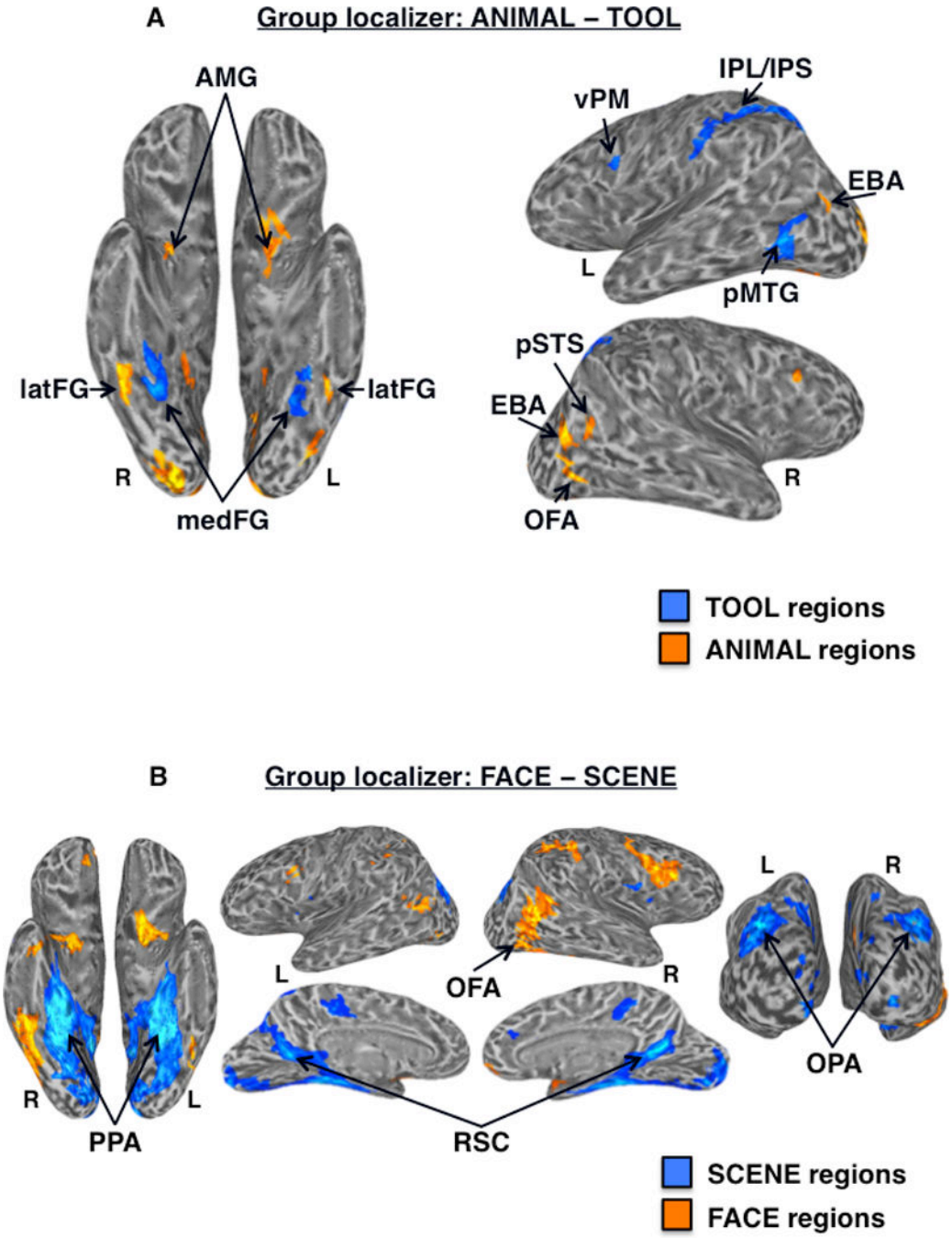

Figure 2.

Group-level functional localizer results. (A) Regions showing significantly higher activation for tools (cool colors) vs. animals (warm colors) in the functional localizer at the group-level (n = 33) displayed on partially inflated ventral (left) and lateral (right) cortical surfaces. TOOL regions included bilateral medFG (VOTC-TOOL) and left pMTG, IPS, IPL, and vPM; ANIMAL regions included bilateral latFG (VOTC-ANIMAL), EBA, AMG, and right OFA and pSTS. (B) Regions showing significantly higher activation for scenes (cool colors) vs. faces (warm colors) in the functional localizer at the group-level (n = 33) displayed on

partially inflated ventral (left), lateral (top middle), medial (bottom middle), and posterior (right) cortical surfaces. SCENE regions included bilateral PPA, RSC, and OPA; the FACE region of interest was the right OFA. Activations are t-statistic maps displayed at node-wise threshold $P < 0.001$; whole-brain threshold $P < 0.01$, FDR corrected; minimum cluster size of 50 nodes. L, left; R, right.

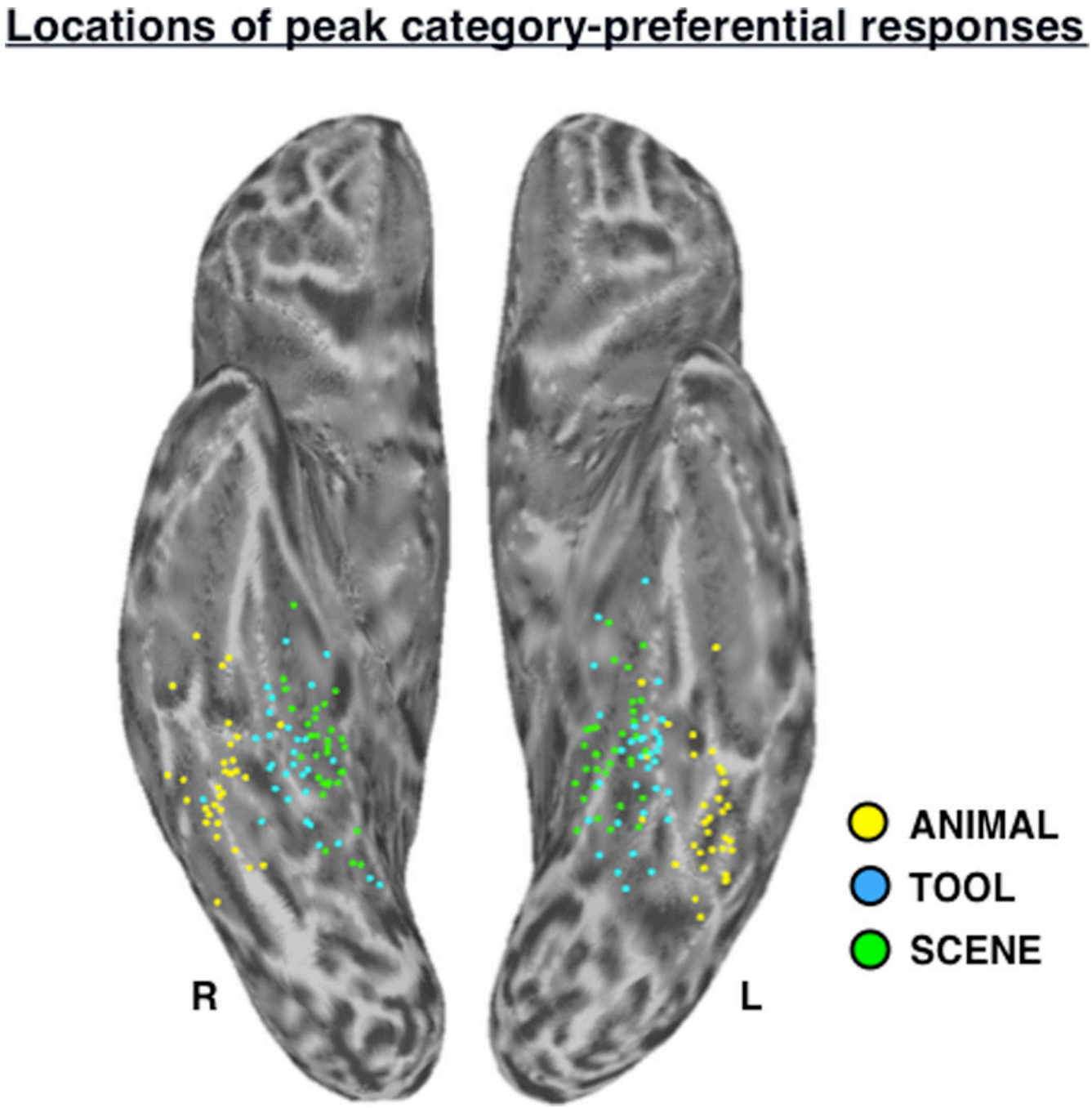

Figure 3.

Locations of peak category-preferential responses in VOTC. Scatter plot depicts the locations of peak SCENE (green dots), TOOL (blue dots), and ANIMAL (yellow dots) activation in the functional localizer contrasts (Table I) for all subjects (n = 33), displayed in standardized surface space on the semi-inflated left and right ventral cortical surfaces. L, left; R, right.

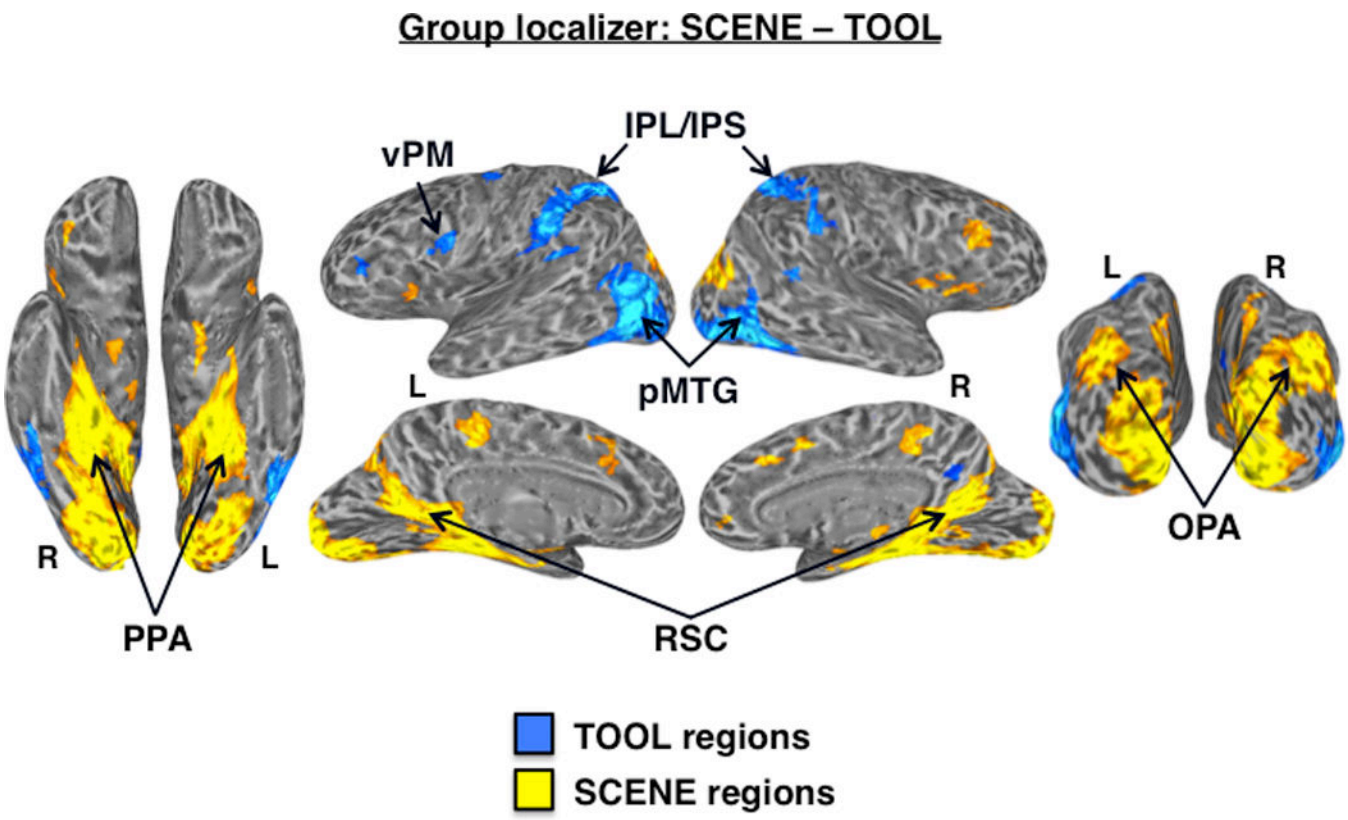

Figure 4.

Differential activation for tools vs. scenes. Group-level functional localizer contrast: SCENE – TOOL. At the standard statistical threshold ($P < 0.001$ nodewise; $P < 0.01$ FDR corrected; minimum cluster size of 50 nodes), there was higher activation for scenes (warm colors) than tools (cool colors) in the bilateral PPA, RSC, and OPA. While there was higher activation for tools than scenes in bilateral pMTG, IPS/IPL, and left vPM, no regions in medial VOTC showed preferential activation for tools at the group-level.

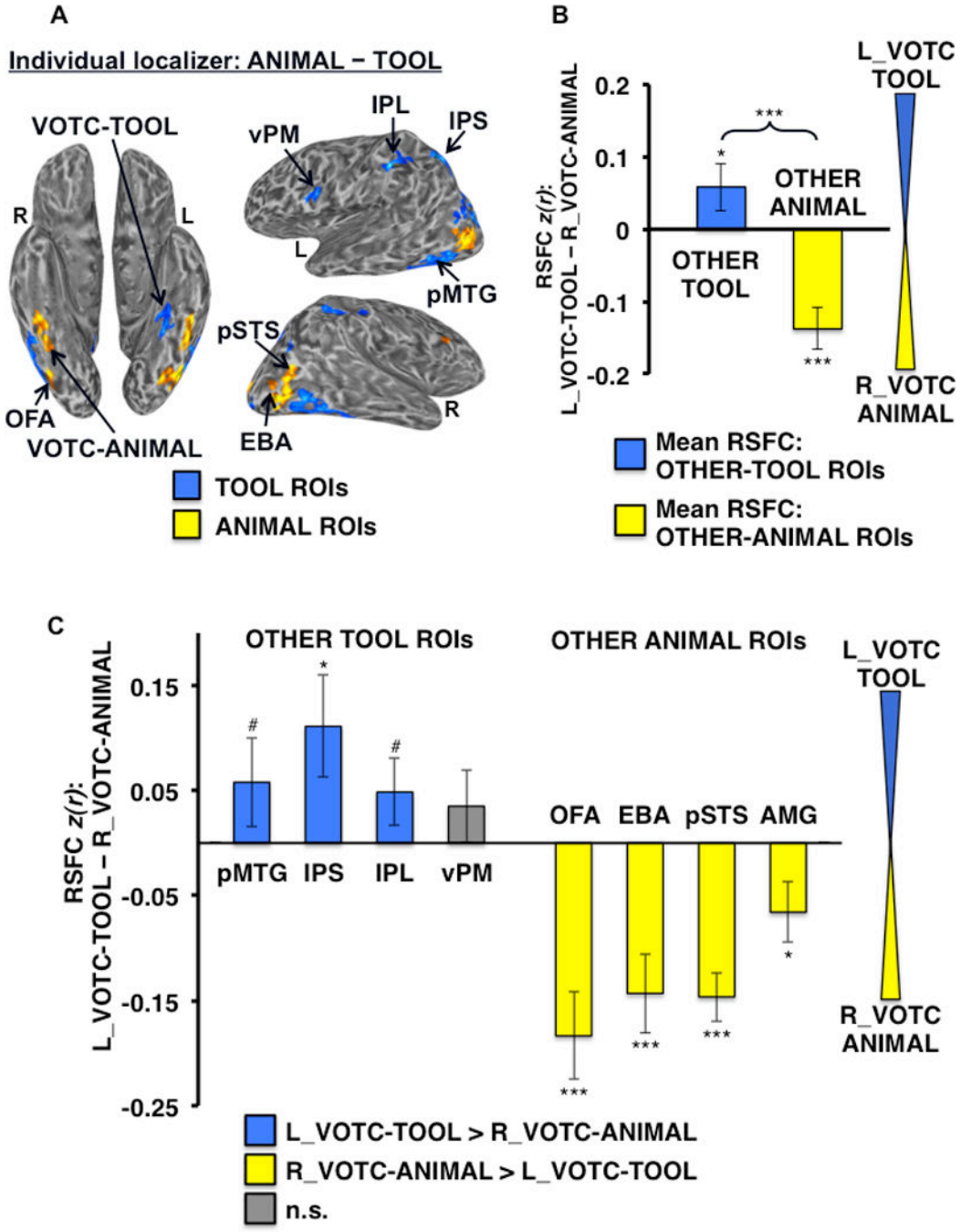

Figure 5.

Differential RSFC of left VOTC-TOOL region and right VOTC-ANIMAL region with OTHER-TOOL vs. OTHER-ANIMAL ROIs. (A) Example individual localizer results displayed on semi-inflated ventral (left) and lateral (right) cortical surfaces. TOOL ROIs included left medFG (VOTC-TOOL), pMTG, IPS, IPL, and vPM; ANIMAL ROIs included right latFG (VOTC-ANIMAL), OFA, EBA, pSTS, and AMG (not apparent for this individual at the given threshold). Activations are tstatistic maps displayed at node-wise threshold $P < 0.001$; whole-brain threshold $P < 0.01$, FDR corrected; minimum cluster size

of 50 nodes). (B) Category-level analysis: Difference in mean RSFC of all OTHER-TOOL regions (blue bar) and all OTHER-ANIMAL regions (yellow bar) with the left VOTC-TOOL vs. right VOTC-ANIMAL region. Positive values indicate stronger mean RSFC with the left VOTC-TOOL region; negative values indicate stronger mean RSFC with the right VOTC-ANIMAL region. The OTHER-TOOL regions showed relatively stronger mean RSFC with the left VOTC-TOOL region; conversely, the OTHER-ANIMAL regions showed relatively stronger mean RSFC with the right VOTC-ANIMAL region. Brace indicates a significant VOTC-ROI (left VOTC-TOOL vs. right VOTC-ANIMAL) by category (OTHER-TOOL vs. OTHER-ANIMAL) crossover interaction. (C) Individual ROI analysis: Difference in RSFC of the individual OTHER-TOOL and OTHER-ANIMAL regions with the left VOTC-TOOL vs. right VOTC-ANIMAL region; positive values (blue bars) indicate stronger RSFC with left VOTC-TOOL region; negative values (yellow bars) indicate stronger RSFC with right VOTC-ANIMAL region; gray bars indicate no significant difference. As predicted, at the individual ROI-level, only OTHER-TOOL ROIs showed stronger RSFC with the left VOTC-TOOL region. Conversely, the ANIMAL ROIs showed stronger RSFC with the right VOTC-ANIMAL region. L, left; R, right; *** $P < 0.001$; * $P < 0.05$; # $P < 0.1$; n.s., not significant. Error bars represent between-subjects s.e.m.

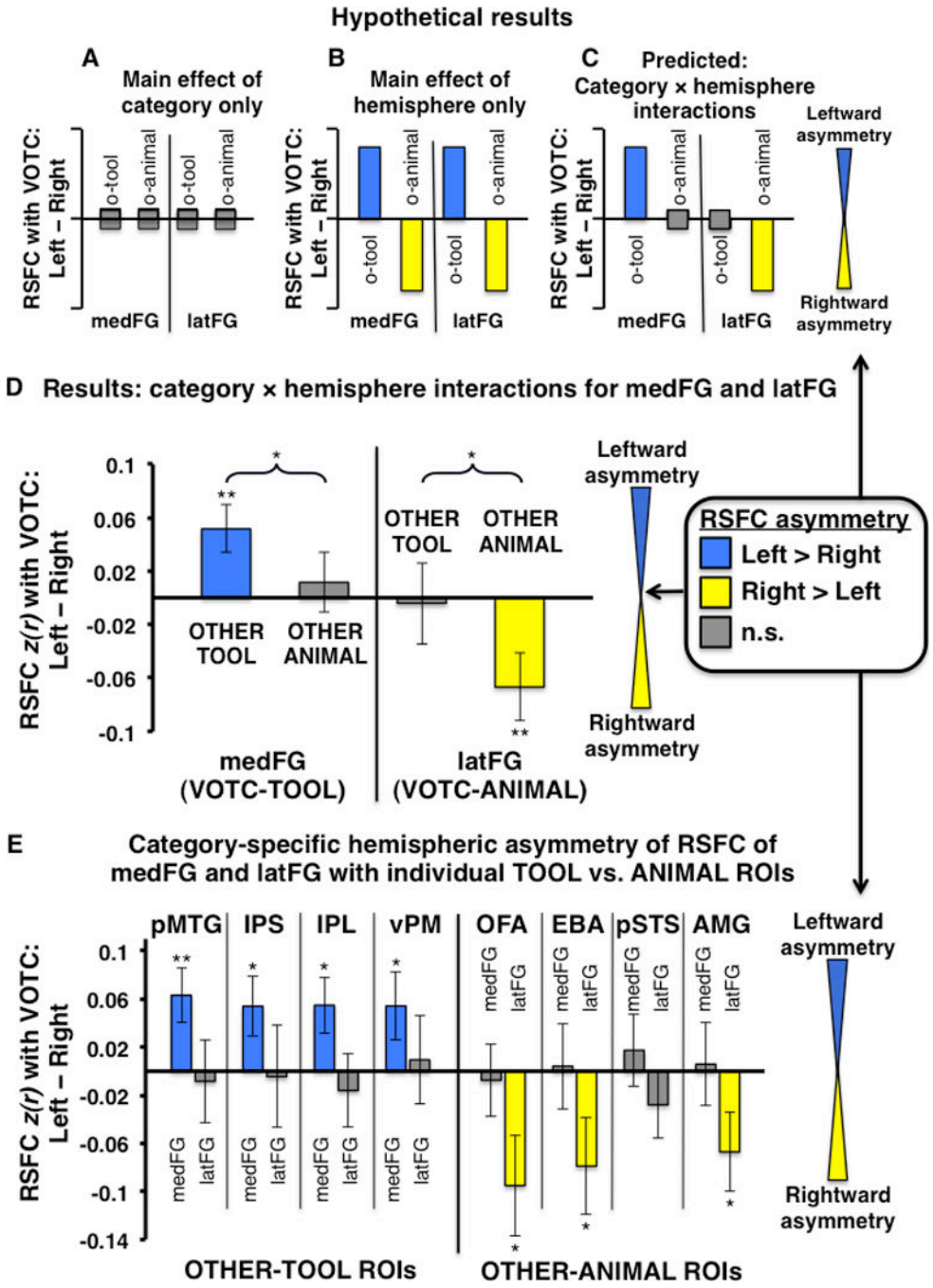

Figure 6.

Category-specific hemispheric asymmetry of VOTC RSFC with OTHER-TOOL and OTHER-ANIMAL regions. (A–E) Plots indicate the degree of hemispheric asymmetry (leftward vs. rightward) of RSFC of homologous VOTC regions with OTHER category-preferential regions; positive values (blue bars) indicate stronger RSFC with the left VOTC-homologue; negative values (yellow bars) indicate stronger RSFC with the right VOTC-homologue; gray bars indicate no significant difference between right and left VOTC RSFC. (A–C) Hypothetical pattern of results expected if there were (A) only a main effect of

category with no hemispheric asymmetry: mean RSFC of both the medFG and latFG with both OTHER-TOOL and OTHER-ANIMAL ROIs would not differ across hemispheres; (B) only a main effect of hemisphere (e.g., RSFC: ipsilateral > contralateral), with no category effect: the left lateralized OTHER-TOOL regions would show stronger mean RSFC with both the left medFG and left latFG relative to their respective homologous regions in the right VOTC, while the right lateralized OTHER-ANIMAL regions would show stronger RSFC with both the right latFG and right medFG relative to their respective homologous regions in the left VOTC; or (C) the predicted VOTC-hemisphere (left vs. right) by category (OTHER-TOOL regions vs. OTHER-ANIMAL regions) interaction for both the medFG and latFG: the OTHER-TOOL regions would show stronger mean RSFC with the left medFG than the right medFG, but the OTHER-ANIMAL regions would show no difference with the left vs. right medFG; conversely, the OTHER-ANIMAL regions would show stronger mean RSFC with the right latFG than the left latFG, but the OTHER-TOOL regions would show no difference with the right vs. left latFG. (D) Group-level analysis: Actual results mirrored the hypothetical predicted results (C), demonstrating leftward asymmetry of medFG RSFC with only OTHER-TOOL regions, but not with OTHER-ANIMAL regions, and conversely, rightward asymmetry of latFG RSFC with only OTHER-ANIMAL regions, but not with OTHER-TOOL regions. (E) Individual ROI analyses: there was leftward asymmetry of RSFC of the medFG with all of the individual TOOL ROIs (IPS, IPL, pMTG, vPM) but no asymmetry of RSFC with any of the ANIMAL ROIs. Conversely, there was rightward asymmetry of RSFC of the latFG with three of four ANIMAL ROIs (OFA, EBA, and AMG) but no asymmetry of RSFC with any of the TOOL ROIs. o-tool, OTHER-TOOL regions; o-animal, OTHER-ANIMAL regions; ** $P < 0.01$; * $P < 0.05$; n.s., not significant. Braces indicate significant VOTC-hemisphere by category interactions; Error bars represent between-subjects s.e.m.

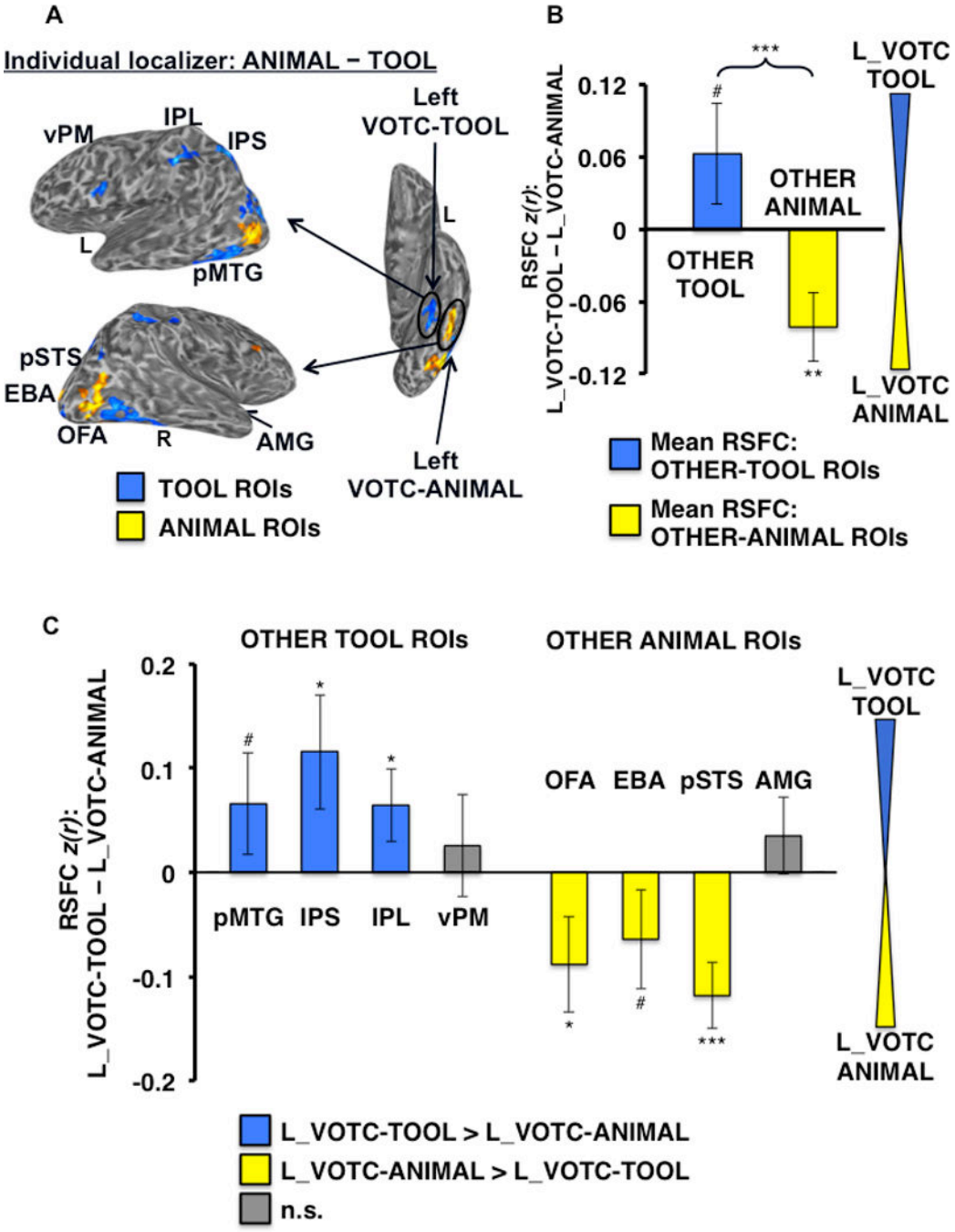

Figure 7.

Differential RSFC of left VOTC-TOOL region and left VOTC-ANIMAL region with OTHER-TOOL vs. OTHER-ANIMAL ROIs. (A) Example individual localizer results displayed on semi-inflated lateral (left) and ventral (right) cortical surfaces, as in Figure 4. Arrows depict the hypothesis that adjacent VOTC-TOOL and VOTC-ANIMAL regions within the left VOTC would show differentially stronger RSFC with OTHER-TOOL vs. OTHER-ANIMAL regions, respectively, when localized at the individual-level. Results of the within-hemisphere analyses at both the category-level (B) and individual ROI-level (C)

are strikingly similar to the parallel cross-hemisphere comparisons (Fig. 5). *** $P < 0.001$; ** $P < 0.01$; * $P < 0.05$; # $P < 0.1$; n.s., not significant All other plots and labels are the same as in Figure 5.

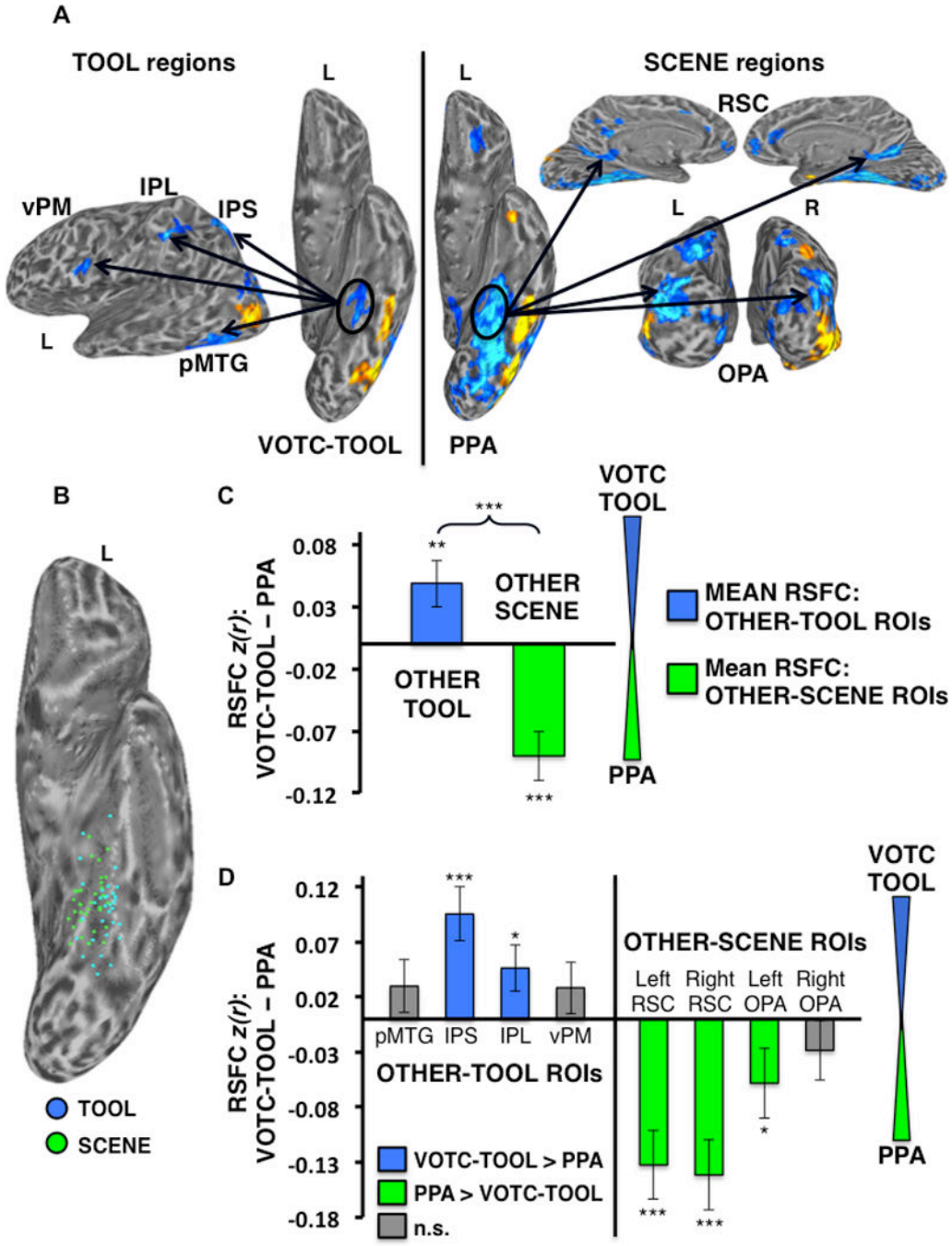

Figure 8.

Differential RSFC of the left VOTC-TOOL region and left PPA with TOOL vs. SCENE ROIs. (A) Example individual localizer: regions showing preferential activation for TOOLS (Contrast: TOOLS > ANIMALS; left) and SCENES (Contrast: SCENES > FACES; right) are displayed (cool colors) on semi-inflated lateral (left) ventral (middle), medial (top right), and posterior (bottom right) cortical surfaces. Activations are t-statistic maps displayed at node-wise threshold $P < 0.001$; wholebrain threshold $P < 0.01$, FDR corrected; minimum cluster size of 50 nodes. Arrows depict the hypothesis that, despite their proximal/

overlapping locations, the VOTC-TOOL region and PPA would show stronger RSFC with OTHER-TOOL vs. OTHER-SCENE regions, respectively, when localized at the individual-level. (B) Scatter plot displays the overlapping spatial distributions of the locations of peak TOOL (blue dots) and SCENE (green dots) activations for all 33 subjects on the partially inflated left ventral cortical surface. (C) Category-level analysis: Difference between the mean RSFC of the OTHER-TOOL ROIs (left pMTG, IPS, IPL, and vPM) and OTHER-SCENE ROIs (bilateral RSC and OPA) with the left VOTC-TOOL region vs. left PPA; positive values indicate stronger mean RSFC with left VOTC-TOOL region; negative values indicate stronger mean RSFC with the left PPA. As predicted, the OTHER-TOOL regions showed relatively stronger mean RSFC with the VOTC-TOOL region; conversely, the OTHER-SCENE ROIs showed relatively stronger mean RSFC with the PPA. Brace indicates a significant VOTC-ROI (VOTC-TOOL region vs. PPA) by category (OTHER-TOOL regions vs. OTHER-SCENE regions) crossover interaction. (D) Individual ROI analysis: Difference between RSFC of the left VOTC-TOOL region vs. left PPA with each of the individual OTHER-TOOL and OTHER-SCENE ROIs; positive values (blue bars) indicate stronger RSFC with the VOTC-TOOL region; negative values (green bars) indicate stronger RSFC with the PPA; gray bars indicate no significant difference. As predicted, only OTHER-TOOL ROIs showed stronger RSFC with left VOTC-TOOL region, including the left IPS and IPL. Conversely, only OTHER-SCENE ROIs showed stronger RSFC with the left PPA, including bilateral RSC and left OPA. L, left; R, right; *** $P < 0.001$; ** $P < 0.01$; * $P < 0.05$; n.s., not significant. Error bars represent between-subjects s.e.m.

Table I

Category-preferential ROI statistics

Contrast	ROI	N	# nodes	size (mm^2)	Peak t-value
tool > animal	**L medFG***	33	119 ± 53	61 ± 25	6.33 ± 1.48
	R medFG*	31	108 ± 43	58 ± 27	6.19 ± 1.83
	L pMTG	18	151 ± 48	75 ± 30	7.26 ± 2.22
	L IPS	27	135 ± 56	63 ± 30	5.31 ± 1.59
	L IPL	30	221 ± 89	68 ± 31	5.83 ± 2.03
	L vPM	28	99 ± 50	58 ± 29	4.51 ± 1.43
animal > tool	**L latFG***	33	136 ± 73	55 ± 29	6.90 ± 2.89
	R latFG*	32	143 ± 52	82 ± 28	8.25 ± 1.99
	R EBA	32	105 ± 46	74 ± 31	8.00 ± 2.72
	R pSTS	29	122 ± 49	52 ± 28	5.19 ± 1.62
	R AMG	15	134 ± 91	27 ± 18	4.19 ± 0.97
face > scene	R OFA	33	161 ± 63	80 ± 26	13.24 ± 3.88
scene > face	**L PPA***	33	171 ± 38	75 ± 17	15.79 ± 3.99
	R PPA*	33	179 ± 27	76 ± 18	16.67 ± 3.16
	L RSC	33	161 ± 51	58 ± 25	8.72 ± 2.51
	R RSC	33	193 ± 35	68 ± 16	10.97 ± 2.81
	L OPA	33	200 ± 74	93 ± 23	13.20 ± 3.48
	R OPA	33	127 ± 45	102 ± 26	13.38 ± 2.99

N, number of subjects with given ROI; All other values represent the mean ± s.d.; L, left; R, right;

*VOTC ROIs